JOURNAL OF PETROLOGY | VOLUME 53 | NUMBER 12 | PAGES 2411–2440 | 2012 | doi:10.1093/petrology/egs054

A New View on the Petrogenesis of the Oman Ophiolite Chromitites from Microanalyses of Chromite-hosted Inclusions

ANASTASSIA Y. BORISOVA[1,2]*, GEORGES CEULENEER[1], VADIM S. KAMENETSKY[3], SHOJI ARAI[4], FRÉDÉRIC BÉJINA[5,6], BÉNÉDICTE ABILY[1], ILYA N. BINDEMAN[7], MIREILLE POLVÉ[1], PHILIPPE DE PARSEVAL[1], THIERRY AIGOUY[1] AND GLEB S. POKROVSKI[1]

[1]GÉOSCIENCES ENVIRONNEMENT TOULOUSE, GET-UMR 5563, OBSERVATOIRE MIDI-PYRÉNÉES, UNIVERSITÉ TOULOUSE III/CNRS/IRD/CNES, 14 AVENUE E. BELIN, 31400 TOULOUSE, FRANCE

[2]GEOLOGICAL DEPARTMENT, LOMONOSOV MOSCOW STATE UNIVERSITY, VOROBIEVI GORI, 119991, MOSCOW, RUSSIA

[3]CODES, ARC CENTRE OF EXCELLENCE IN ORE DEPOSITS, UNIVERSITY OF TASMANIA, HOBART, TAS. 7001, AUSTRALIA

[4]DEPARTMENT OF EARTH SCIENCES, KANAZAWA UNIVERSITY, KANAZAWA 920-1192, JAPAN

[5]UNIVERSITÉ DE TOULOUSE III, UPS-OMP, IRAP, TOULOUSE, FRANCE

[6]CNRS, INSTITUT DE RECHERCHE EN ASTROPHYSIQUE ET PLANÉTOLOGIE, IRAP, 14 AVENUE E. BELIN, 31400 TOULOUSE, FRANCE

[7]GEOLOGICAL SCIENCES, UNIVERSITY OF OREGON, 1275 E 13TH STREET, EUGENE, OR, USA

RECEIVED NOVEMBER 2, 2011; ACCEPTED JULY 16, 2012
ADVANCE ACCESS PUBLICATION SEPTEMBER 12, 2012

To decipher the petrogenesis of chromitites from the Moho Transition Zone of the Cretaceous Oman ophiolite, we carried out detailed scanning electron microscope and electron microprobe investigations of ~500 silicate and chromite inclusions and their chromite hosts, and oxygen isotope measurements of seven chromite and olivine fractions from nodular, disseminated, and stratiform ore bodies and associated host dunites of the Maqsad area, Southern Oman. The results, coupled with laboratory homogenization experiments, allow several multiphase and microcrystal types of the chromite-hosted inclusions to be distinguished. The multiphase inclusions are composed of micron-size (1–50 μm) silicates (with rare sulphides) entrapped in high cr-number [100Cr/(Cr + Al) up to 80] chromite. The high cr-number chromite coronas and inclusions are reduced (oxygen fugacity, f_{O2}, of ~3 log units below the quartz–fayalite–magnetite buffer, QFM). The reduced chromites, which crystallized between 600 and 950°C at subsolidus conditions, were overgrown by more oxidized host chromite ($f_{O2} \approx$ QFM) in association with microcrystal inclusions of silicates (plagioclase An_{86}, clinopyroxene, and pargasite) that were formed between 950 and 1050°C at 200 MPa from a hydrous hybrid mid-ocean ridge basalt (MORB) melt. Chromium concentration profiles through the chromite coronas, inclusions, and host chromites indicate non-equilibrium fractional crystallization of the chromitite system at fast cooling rates (up to ~0·1°C a^{-1}). Oxygen isotope compositions of the chromite grains imply involvement of a mantle protolith (e.g. serpentinite and serpentinized peridotite) altered by seawater-derived hydrothermal fluids in an oceanic setting. Our findings are consistent with a three-stage model of chromite formation involving (1) mantle protolith alteration by seawater-derived hydrothermal fluids yielding serpentinites and serpentinized harzburgites, which were probably the initial source of chromium, (2) subsolidus crystallization owing to prograde metamorphism, followed by (3) assimilation and fractional

*Corresponding author. Present address: GET, UMR 5563, 14 Avenue E. Belin, 31400 Toulouse, France. Telephone: +33(0)5 61 33 26 31. Fax: +33(0)5 61 33 25 60. E-mail: anastassia.borisova@get.obs-mip.fr

crystallization of chromite from water-saturated MORB. This study suggests that the metamorphic protolith assimilation occurring at the Moho level may dramatically affect MORB magma chemistry and lead to the formation of economic chromium deposits.

KEY WORDS: *Oman ophiolite; chromitite; chromian spinel; MORB; inclusions; Moho Transition Zone; hydrothermal fluid; serpentinites; protolith; oxygen isotopes; AFC*

INTRODUCTION

Chromian spinel in the mantle–crust transition zone (referred to here as the Moho Transition Zone or MTZ) plays an important role in the global budget of chromium in the Earth's lithosphere. The chemical composition of chromian spinel and chromite-hosted inclusions is variable, reflecting the wide range of physicochemical and geological conditions that can exist along the interface between the crust and upper mantle (e.g. Dick & Bullen, 1984; Roeder & Reynolds, 1991; Sack & Ghiorso, 1991; Kamenetsky, 1996; Borisova *et al.*, 1997, 2002, 2008; Kamenetsky *et al.*, 2001; Arai *et al.*, 2006). Chromian spinel is a main economic Cr reserve on Earth and may form large chromitite ore bodies whose petrogenesis remains a subject for debate. The pioneering model of McDonald (1965) on the Bushveld chromitites invoked the formation of Cr-rich immiscible liquids, forming at temperatures above 1400°C and even as high as 2000°C (Jackson, 1966). However, this model cannot be applied to chromitites in ophiolites or layered intrusions where hydrous silicate minerals, crystallizing at much lower temperatures, are systematically found as inclusions in chromite (e.g. Lorand & Ceuleneer, 1989; Melcher *et al.*, 1997; Li *et al.*, 2005; Arai *et al.*, 2006; Pagé *et al.*, 2008; Rollinson, 2008). Other models were subsequently proposed to explain chromitite petrogenesis based on experimental data (e.g. Roeder & Reynolds, 1991), chromite-hosted inclusion data (e.g. Melcher *et al.*, 1997; Schiano *et al.*, 1997; Li *et al.*, 2005; Spandler *et al.*, 2005; Borisova *et al.*, 2008), or both (e.g. Irvine, 1975; Matveev & Ballhaus, 2002). Most models invoke a magmatic system, based on experimental data on basaltic systems (e.g. Irvine, 1975; Murck & Campbell, 1986; Roeder & Reynolds, 1991; Matveev & Ballhaus, 2002). For example, Irvine (1975) suggested either crustal contamination or silicate melt mixing to stabilize chromite on the liquidus in such a system. Roeder & Reynolds (1991) suggested a highly reduced basaltic magma as the chromium source. Matveev & Ballhaus (2002) proposed a magmatic system saturated with an aqueous fluid phase with physical separation of chromite from olivine. These models consider either open-system interactions of olivine-saturated melts with felsic melts (Irvine, 1975) or incongruent dissolution of crustal rocks with the formation of chromite-saturated melts (Bédard *et al.*, 2000). Hydrous magmas are indeed favourable for abundant chromite crystallization because the presence of water in a mafic melt widens the stability domain of spinel, especially under oxidizing conditions (Ford *et al.*, 1972; Feig *et al.*, 2006) and stabilizes chromite on the liquidus (Nicholson & Mathez, 1991). However, a major shortcoming of most previous models is the lack of a satisfactory explanation for the source of the Cr capable of accounting for the formation in a mid-oceanic ridge setting of huge chromitite ore bodies reaching tens of thousand cubic meters (e.g. Lorand & Ceuleneer, 1989).

Most researchers acknowledge the role of aqueous fluids or hydrous silicate melts in the petrogenesis of the Oman chromitites (Johan *et al.*, 1983; Augé, 1987; Lorand & Ceuleneer, 1989; Leblanc & Ceuleneer, 1992; Schiano *et al.*, 1997; Arai *et al.*, 2004, 2006; Ahmed *et al.*, 2006; Rollinson, 2008). The source of water and its involvement in the Maqsad MTZ chromitite petrogenesis is, however, controversial. Water might originate from either (1) hydrothermal fluid sources (Augé & Johan, 1988) or (2) dehydration of a subducting slab (Schiano *et al.*, 1997; Ahmed *et al.*, 2006; Rollinson, 2008) or (3) re-melting of hydrated lithosphere in a spreading-ridge setting in response to episodic emplacement of mantle diapirs at the MTZ (Benoit *et al.*, 1999; Python *et al.*, 2007).

Studies of inclusions trapped in chromian spinel crystals may provide key information on the petrogenesis of chromitite ore bodies. Chromian spinel is an ideal 'microcontainer' for inclusions owing to its resistance to alteration (e.g. Shimizu *et al.*, 2001; Arai *et al.*, 2006, 2011). In contrast to chromites disseminated in volcanic rocks (Kamenetsky, 1996; Borisova *et al.*, 2001; Kamenetsky *et al.*, 2001, 2002), chromian spinel forming chromitite ores contains abundant inclusions of fluid, hydrous and anhydrous silicates, sulphides, and platinum group minerals (Augé, 1987; Augé & Johan, 1988; Lorand & Ceuleneer, 1989; Melcher *et al.* 1997; Kamenetsky *et al.*, 2001, 2002; Arai *et al.*, 2004; Spandler *et al.*, 2005; Ahmed *et al.*, 2006; Borisova *et al.*, 2008). Inclusions of hydrous silicate minerals have been found in chromian spinel from chromitites in different tectonic settings, ranging from subduction zones to spreading ridges, and in their fossil equivalents exposed in ophiolites (e.g. Lorand & Ceuleneer, 1989; Melcher *et al.*, 1997; Arai *et al.*, 2006; Rollinson, 2008). However, the origin of these hydrous silicate minerals and the role of aqueous fluids and/or hydrous melts in chromite petrogenesis remain unclear.

We carried out a systematic investigation by scanning electron microscope and electron microprobe of about 500 chromite-hosted inclusions and their host chromites as well as oxygen isotope measurements of chromite and olivine grain fractions from four nodular, disseminated, and stratiform chromitites and three associated host dunites located at different levels of the MTZ in the Oman

ophiolite, Maqsad area. We also performed homogenization experiments on the chromite-hosted inclusions, and analysed numerous elemental profiles through inclusion–host interfaces. The new data are evaluated with existing petrogenetic models and imply that metamorphic recrystallization of a mantle protolith altered by seawater-derived hydrothermal fluids is likely to be the key process responsible for the formation of chromitite ore in an oceanic MTZ setting.

GEOLOGICAL BACKGROUND AND SAMPLES

The Maqsad area of the Oman ophiolite

The Oman ophiolite is an ~95–100 Ma fragment of the Tethyan oceanic lithosphere obducted onto Arabian continental lithosphere (Coleman, 1981; Tilton *et al.*, 1981; Tippit *et al.*, 1981). It was detached during an intra-oceanic thrusting event that occurred ~95 Myr ago; that is, soon after its igneous accretion (Ghent & Stout, 1981; Boudier *et al.*, 1985, 1988; Montigny *et al.*, 1988). The final emplacement onto the Oman margin was achieved during Maastrichtian times (~70 Ma) (Glennie *et al.*, 1973; Coleman, 1981). The present exposure of the Oman ophiolite results from the recent (Miocene) uplift of the Oman range (Glennie *et al.*, 1973). The detailed context of the petrogenesis and emplacement of the Oman ophiolite is still debated. It may have evolved in a mid-ocean ridge setting (e.g. Coleman, 1981) or in a marginal, possibly back-arc, setting (e.g. Pearce *et al.*, 1981; Searle & Cox, 1999; Tamura & Arai, 2006).

Maqsad mantle diapir

The Maqsad area is located in the southeastern part of the Oman ophiolite (Fig. 1). Its structural and igneous evolution was conditioned by the emplacement of a mantle diapir at Moho level below a spreading axis (Jousselin *et al.*, 1998; Rabinowicz & Ceuleneer, 2005). The Maqsad mantle diapir is less than 10 km in cross-section but constitutes the central part of a much larger structure: a former spreading segment, about 80 km in length parallel to the paleo-spreading axis (which trends NW–SE). Abundant primitive melts percolated through the mantle peridotite in the diapir and are now manifested by troctolitic and gabbroic 'impregnations' and segregations (Python & Ceuleneer, 2003; and references therein). The parental melts of the Maqsad troctolites and gabbros were similar to mid-ocean ridge basalt (MORB) as attested by the crystallization sequence and mineral composition (Kelemen *et al.*, 1995; Python *et al.*, 2008; and references therein). Their isotopic signature is typically that of present-day Indian MORB, pointing to a common mantle source (Benoit *et al.*, 1999; and references therein).

The crustal section at the top of the Maqsad diapir is made of flat-lying, slightly dipping to the SE, interlayered cumulates such as dunites, troctolites, olivine gabbros and gabbros, presenting variably developed modal graded bedding. The thickness of this gabbroic unit reaches about 2 km. The overlying sheeted dykes have a NW–SE azimuth. The regularity of the gabbro layering is locally perturbed by syn-magmatic normal faults (Abily *et al.*, 2011). The petrological nature of MORB-derived segregations in the mantle peridotite that were 'processed' in the Maqsad diapir contrasts with the more common situation observed in Oman where mantle dykes are essentially filled with pyroxenite and high-Mg gabbronorite (Python & Ceuleneer, 2003). The parental melts of the Oman pyroxenites and gabbronorites are interpreted to have been formed by low-pressure hydrous re-melting of the hydrated oceanic lithosphere in a mid-ocean ridge setting (Benoit *et al.*, 1999; Clénet *et al.*, 2010). Such pyroxenites and gabbronorites are absent from the Maqsad diapir but occur as intrusions in the mantle peridotite and as layered lower crustal cumulates 10–15 km away from the Maqsad diapir. These pyroxenites and gabbronorites are possibly relics of shallow lithospheric melts that formed in the early stages of the opening of the Maqsad basin, and that were eventually transported passively into an off-axis position by sea-floor spreading (Benoit *et al.*, 1999; Clénet *et al.*, 2010).

Signatures of hydrothermal activity

Evidence for deep and very hot (up to at least 900°C) hydrothermal activity is strong in the Maqsad area. It is manifested by veins (usually ridge-parallel) filled with hydrothermal diopside and anorthite (Python *et al.*, 2007), peridotites transformed into assemblages of talc and carbonates, and igneous minerals (cumulates from the lower crust) partially transformed into amphibole and green spinel in the vicinity of syn-magmatic faults (Abily *et al.*, 2011). These are the footprints of transient interaction processes between the hot basaltic melts percolating through the Maqsad diapir and filling the magma chamber and hydrothermal fluids reaching the Moho level. More classical lower-temperature minerals and their mineral assemblages (serpentine, chlorite, tremolite, sulphide, sulphate, carbonate and zeolite) are also abundant in faults and cracks withn the Maqsad mantle and lower crustal sections (Abily *et al.*, 2011; and references therein). This hydrothermal activity has led locally to the formation of small plagiogranitic pods (Amri *et al.*, 1996, see also Koepke *et al.*, 2007).

Maqsad Moho Tranzition Zone (MTZ)

The transition between the layered gabbroic cumulates and the underlying mantle harzburgites is represented by an ~300 m thick dunitic transition zone. The dunitic rocks are particularly well developed above the center of the Maqsad mantle diapir (Fig. 2). Chromitite ore bodies,

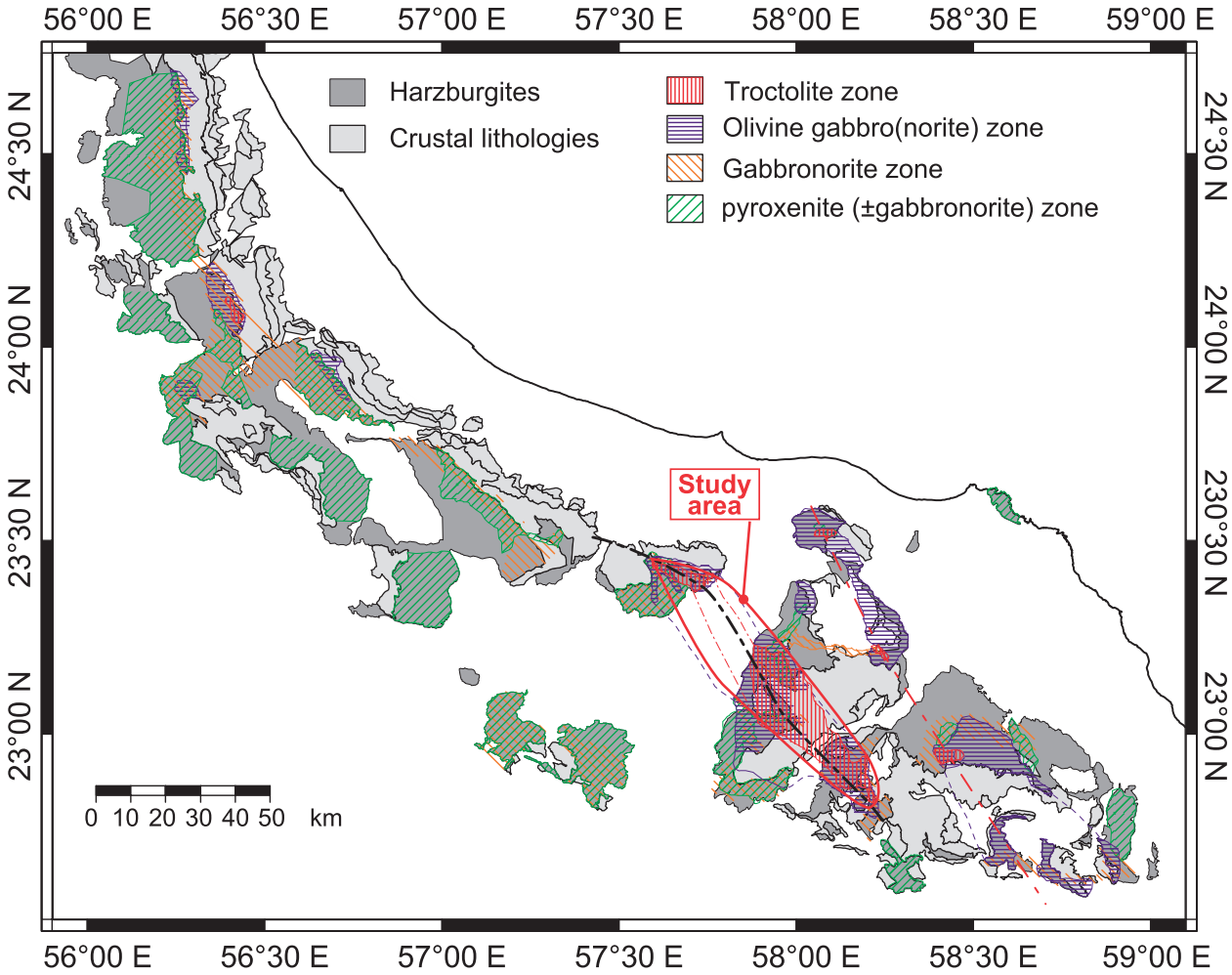

Fig. 1. Map of the Oman ophiolite showing the location of the Maqsad study area. Troctolites are MORB cumulates developed above and within the Maqsad diapir surface area (~1000 km^2). There are numerous occurrence of evolved lithospheric cumulates (gabbronorites and pyroxenites) near the Maqsad area (marked by orange and green shading). Modified after Python & Ceuleneer (2003).

which are the focus of the present study, are abundant in the Maqsad dunitic transition zone (Leblanc & Ceuleneer, 1992). They were neither deformed nor transposed by mantle solid-state flow, unlike most of the chromitite ore bodies cropping out in the mantle harzburgites. This good preservation of the Maqsad chromitite bodies offers a unique opportunity to study in detail the magmatic processes related to chromite ore genesis. Our study focuses on the undeformed chromitites, which are among the most spectacular manifestations of complex processes in the MTZ. The chromitite samples investigated come from three ore bodies located at various levels in the MTZ above the Maqsad diapir (Fig. 2).

Host dunites

The host dunite samples are predominantly composed of olivine (>95% of olivine, Fo 87·5–90·5 mol %), scattered chromian spinel (cr-number varies from 32 to 55) and interstitial diopside (Abily & Ceuleneer, in press). The investigated samples are weakly altered (≤30% serpentine) dunites (11TUF1: 23°6'16·86"N, 57°57'58·44"E, 883 m; 11TUF2: 23°6'15·96"N, 57°58'3·78"E, 898 m) and diopside-bearing dunite (11TUF7: 23°6'9·54"N, 57°58'28·26"E, 977 m) hosting the chromitites at the Maqsad MTZ. The dunite samples consist of partly serpentinized olivine (Fo 87–89 mol %), scattered chromite (cr-number = 50–54) and interstitial diopside (mg-number ~96).

Stratiform chromitite

Sample 04 OM 31 E is from a stratiform chromitite body at the base of the MTZ (23°07.055N, 57°56.618E, 950 m). This body is about 45 m thick and consists of interlayered horizons of massive ore (>90% chromite) up to 3 m in thickness and of disseminated ore. The massive ore is a

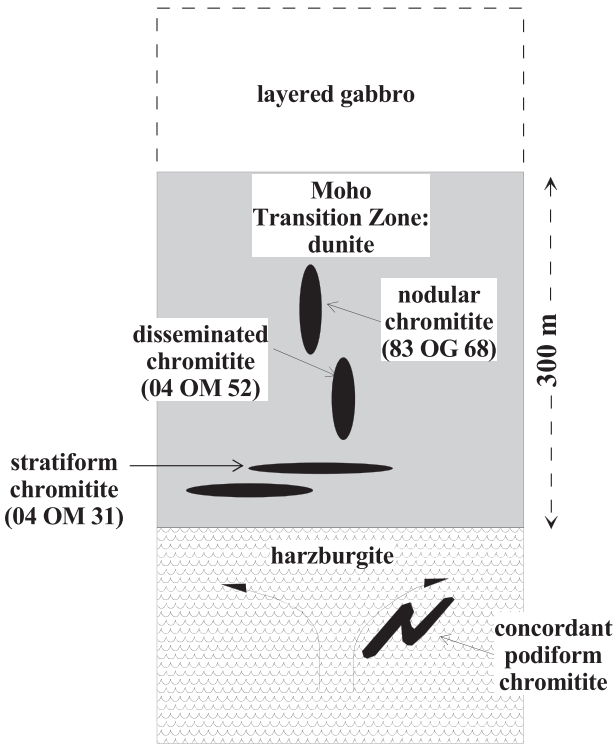

Fig. 2. Schematic geological cross-section of the Moho Transition Zone (MTZ) in the Maqsad area of the Oman ophiolite. Chromitite ore bodies are localized in the host dunite layer (~300 m thickness).

compact assemblage of euhedral to subhedral chromite grains 100–200 μm in size; the interstitial silicate minerals are olivine, diopside, pargasite and, rarely, enstatite. The disseminated ore exhibits antinodular textures (nodular aggregates of olivine grains embedded in a matrix of chromian spinel) or, more commonly, chain textures (subhedral single olivine grains with interstitial chromian spinel). These textures suggest that a partly consolidated dunitic host was invaded and partly disaggregated by a hydrated melt that precipitated chromian spinel (± other silicate minerals) (e.g. Bédard *et al.*, 2007). The chromian spinel to olivine ratio exhibits gradual variations, defining graded bedding. This indicates that the stratiform chromitite formed a suspension at some stage of its evolution. Chromite grains contain silicate and chromite inclusions (Table 1).

Disseminated chromitite

Sample 04 OM 52D from a disseminated chromitite of the median part of the dunitic MTZ (23°05.703N, 57°57.675E, 997 m) where irregular patches of interstitial chromian spinel (locally concentrated to form lenses of massive ore) are abundant and interpreted as former magmatic impregnations (Leblanc & Ceuleneer, 1992). The silicate minerals are olivine, clinopyroxene, pargasite, and plagioclase.

Nodular chromitite

Two samples of nodular chromitite [83 OG 68(1) and 83 OG 68(2)] come from an ~3 m thick and ~35 m high dyke located at the top of the MTZ (23°06.013N, 57°58.601E, 1225 m), several tens of meters below the layered gabbros. Troctolitic and gabbroic sills are present in the dunite that hosts the dyke. The dyke is vertical and strikes parallel to the paleo-ridge axis (NW–SE). The contact between the chromite ore filling the dyke and the host dunite is sharp. The texture of the ore is nodular. Chromitite nodules may reach 2 cm in size. They consist of sintered aggregates of minute (a few hundred micrometres) chromite grains containing silicate inclusions (Table 1). A nucleus rich in silicates (olivine, clinopyroxene, plagioclase) is often present in the core of the nodules. At the base of the dyke [83 OG 68(1)], the nodules are tightly packed and flattened. The size and abundance of the nodules decrease progressively upward, and the texture of the ore becomes disseminated [single chromian spinel grains embedded in a silicate matrix, 83 OG 68(2)] at the top of the dyke. This chromitite ore body is pervasively affected by hydrothermal alteration, primary magmatic minerals from the silicate matrix (olivine, clinopyroxene and plagioclase) being partly transformed into low-temperature hydrous minerals such as serpentine, chlorite, prehnite and zeolites (Leblanc & Ceuleneer, 1992). Carbonates are also commonly found as alteration products.

Sample preparation and analyses

We selected samples that had escaped pervasive transformation of the primary silicate assemblage into low-temperature hydrothermal phases. The freshest samples still contain some minor secondary minerals (≤5%) such as tremolite, hydrogrossular, talc, chlorite, carbonate and serpentine (in dunites) and sulphides scattered between and inside the primary grains along cracks and replacing the primary silicate phases. A database of all the studied silicate and chromite phases, including the host chromite and minerals of the chromite-hosted inclusions (Table 1), is available in the Electronic Appendix (EA; available for downloading at http://www.petrology.oxfordjournals.org).

Different inclusion types were identified based on detailed backscattered electron images of about 200 inclusions in four samples of nodular, disseminated and stratiform chromitite using a scanning electron microscope [JEOL JSM-6360 LV at Geosciences Environment Toulouse (GET), France and JEOL JSM-6480LV with EDS INCA-Energy 350 at Geological Department of Moscow State University, Moscow, Russia]. Major and minor element concentrations in the minerals of the inclusions and their host spinel were determined by electron microprobe using a CAMECA SX50 microprobe (GET)

Table 1: Types of chromite-hosted inclusions of nodular, disseminated and stratiform chromitites of the Maqsad MTZ (Oman ophiolite)

Type	Shape	Mineralogical composition	Features of inclusion	Sample number	Figure	Participating melt or fluid
Multiphase assemblage						
1	Rounded or lens-shaped	Cr-Na Parg ± Enst ± Cpx ± Sulph as co-entrapped phases*	Cr-Na Parg overgrowths on Enst; associated with Chr coronas	Nodular: 83 OG 68(2)	4b	Aqueous fluid
2	Rounded or octahedral shape	Aspid ± Enst ± Cr-Na Parg ± Sulph	Aspid is the predominant mineral in inclusion; Aspid overgrowths on Enst and Cr-Na Parg; associated with Chr coronas	Nodular: 83 OG 68(1) Disseminated: 04 OM 52D	4d, 5a	Aqueous fluid
2a	Octahedral shape	Aspid/Phlog/Cr-Na Parg ± Enst ± Sulph, rare Serp, altered spinel	Aspid/Phlog/Cr-Na Parg are associated with Chr coronas; predominant type in the stratiform chromitite 04 OM 31E	Disseminated: 04 OM 52D Stratiform: 04 OM 31E	4c, 5b and f	Aqueous fluid
Microcrystal(s)						
3	Euhedral Anhedral	Enst + Cpx, Fo	Euhedral, anhedral as associated with Chr coronas	Nodular: 83 OG 68(2) Disseminated: 04 OM 52D	4e, 5e	Aqueous fluid
4	Anhedral	Cpx/Plag ± Cr-Na Parg	Microcrystals are isolated or associated; Trem as replacing Plag	Nodular: 83 OG 68(1) 83 OG 68(2) Disseminated: 04 OM 52D	4f	Hydrous hybrid MORB
5	Anhedral Euhedral	Hgross ± Cr-Na Parg	Isolated crystals; Hgross as replacing Plag	Nodular: 83 OG 68(2)	4g	Hydrous hybrid MORB
6	Euhedral	Chr	Isolated primary crystals; frequent association with hydrous silicate micro-inclusions	Disseminated: 04 OM 52D	4h, 5c and d	Aqueous fluid

Aspid, aspidolite; Cpx, clinopyroxene (between augite and diopside composition); Plag, plagioclase; Chr, chromite with high cr-number (chromite phase visible with optical microscopy in type 2a and invisible in type 2 inclusions); Cr-Na Parg, Cr-Na pargasite; Enst, enstatite; Fo, forsterite; Hgross, hydrogrossular; Phlog, phlogopite (in stratiform chromitites); Sulph, sulphides; Trem, tremolite replacing plagioclase; Serp, serpentine (in stratiform chromitites).
*Fe-Ni and Os-Ru-Ir sulphide microphases (laurite–erlichmanite group) are identified in the type 1, 2 and 2a multiphase inclusions.

with SAMX automation and wavelength-dispersive spectrometry (WDS). Analyses were conducted using an accelerating voltage of 15 kV, a beam current of 10 nA for silicate minerals and 20 nA for chromian spinels, and a beam size of 2 μm. The applied acquisition conditions are typical for standard electron microprobe analysis (e.g. Borisova *et al.*, 2010), allowing low detection limits (300–700 ppm for most major and minor elements in chromite and ~1200 ppm for Ni) and high internal precision (RSD ≤3% for major Mg, Al, Cr and Fe, and ≤30% for minor Mn and Ti in chromite). The compositions are reported in Figs 3–6, Table 2 and the Electronic Appendix. The ferric iron content of the chromite was determined by assuming ideal stoichiometry, XY_2O_4, where $X = (Fe^{2+}, Mg, Ni, Mn, Co, Zn)$ and $Y = (Cr^{3+}, Fe^{3+}, Al)$. Titanium is assumed to be present as an ulvöspinel component, and Cr as Cr^{3+}. Iron is subdivided into ferrous and ferric to satisfy the condition $n_Y = 2 \times n_X$, where n_Y is the total number of trivalent cations and n_X is the total number of divalent cations per unit cell. Possible Cr^{2+} contents in chromite are negligible because only Cr^{3+} is a major component stabilizing chromian spinel (Hanson & Jones, 1998).

The large size of the chromite crystals and aggregates makes them ideal targets for high-precision analyses by

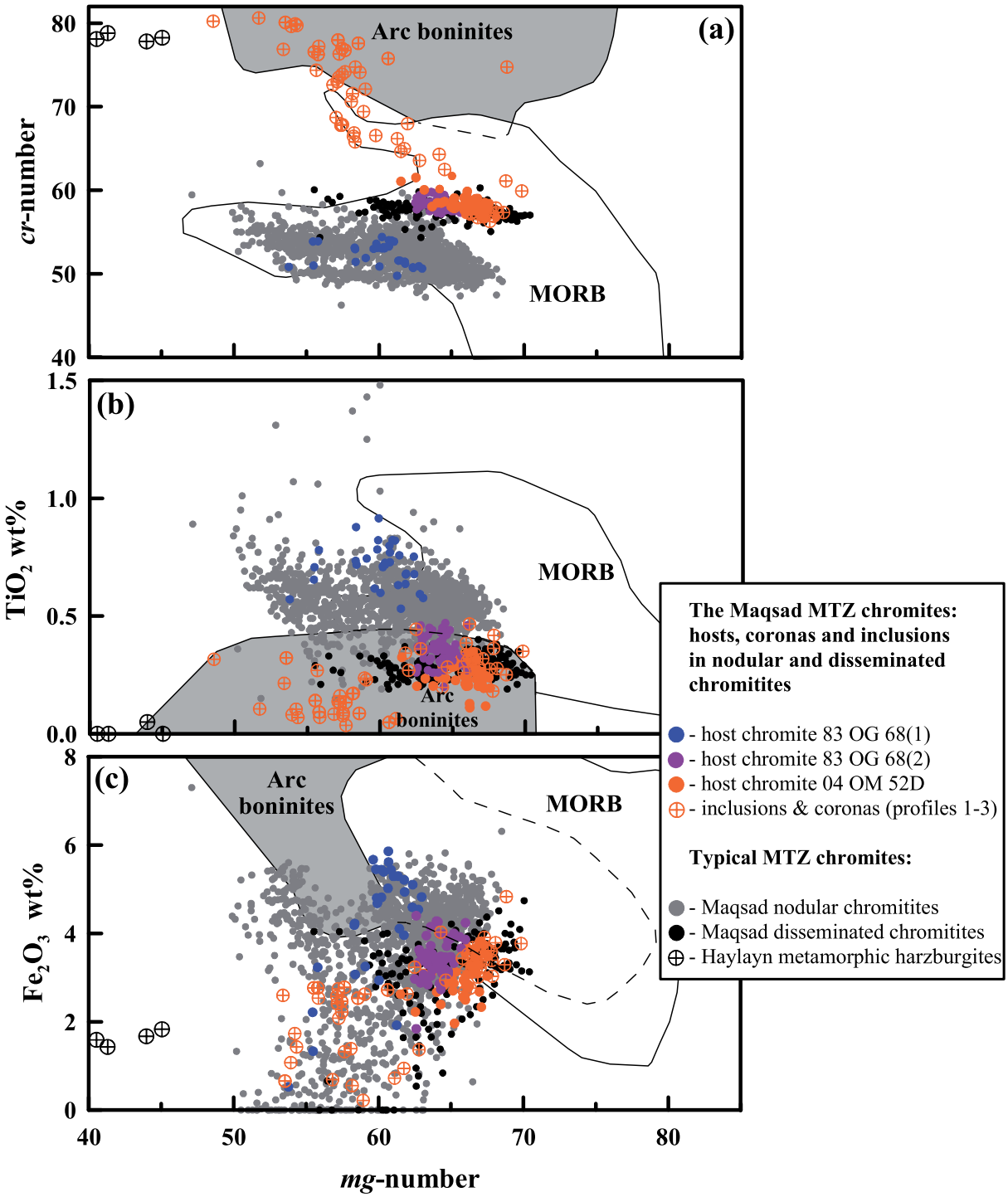

Fig. 3. (a–c) Cr-number [100Cr/(Cr + Al)], TiO_2 and Fe_2O_3 contents vs mg-number [100 Mg/(Mg + Fe^{2+})] of the host chromite, chromite coronas and inclusions in nodular and disseminated chromitites of the Maqsad MTZ of the Oman ophiolite. Chromite data are summarized in Table 2 and the Electronic Appendix. The data for 'Haylayn metamorphic harzburgites' correspond to chromites from the serpentinized peridotites of the Haylayn area (G. Ceuleneer, unpublished data). The typical Maqsad MTZ chromite compositions are according to G. Ceuleneer (unpublished data). The 'MORB' field corresponds to chromite compositions from http://www.petdb.org (Lehnert *et al.*, 2000) and data summarized by Kamenetsky *et al.* (2001, 2002); 'Arc boninites' are chromite compositions from Sigurdsson *et al.* (1993) and Kamenetsky *et al.* (2001, 2002) and the chromite database of Barnes & Roeder (2001). (d–f) Cr-number [100Cr/(Cr + Al)], TiO_2 and Fe_2O_3 contents vs mg-number [100 Mg/(Mg + Fe^{2+})] of the host chromite and chromite coronas in the Maqsad stratiform chromitites of the Oman ophiolite. The 'MORB' field and 'Arc boninitic series' or 'Arc boninites' field are shown for comparison. All data sources are as in (a–c).

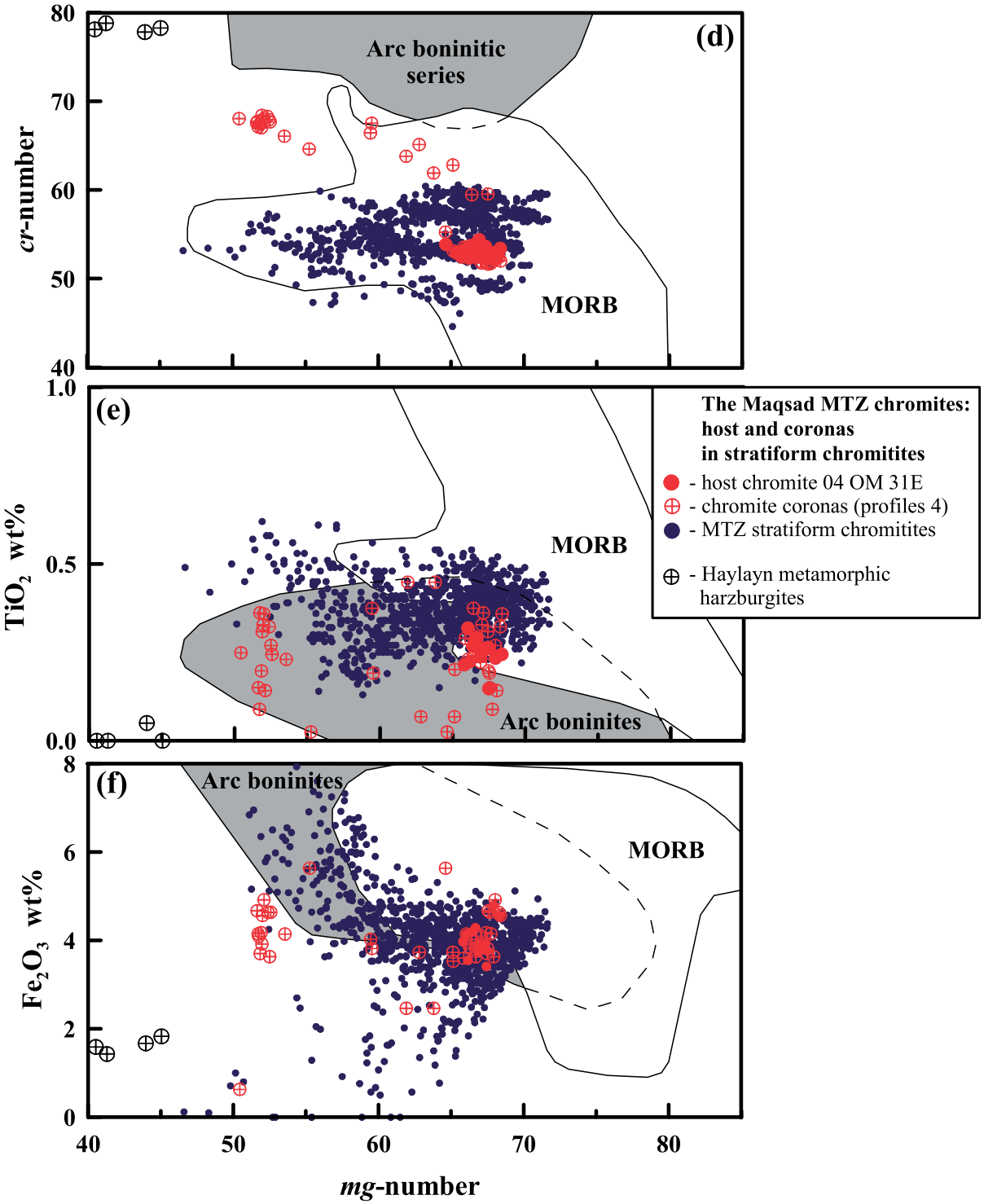

Fig. 3. (Continued)

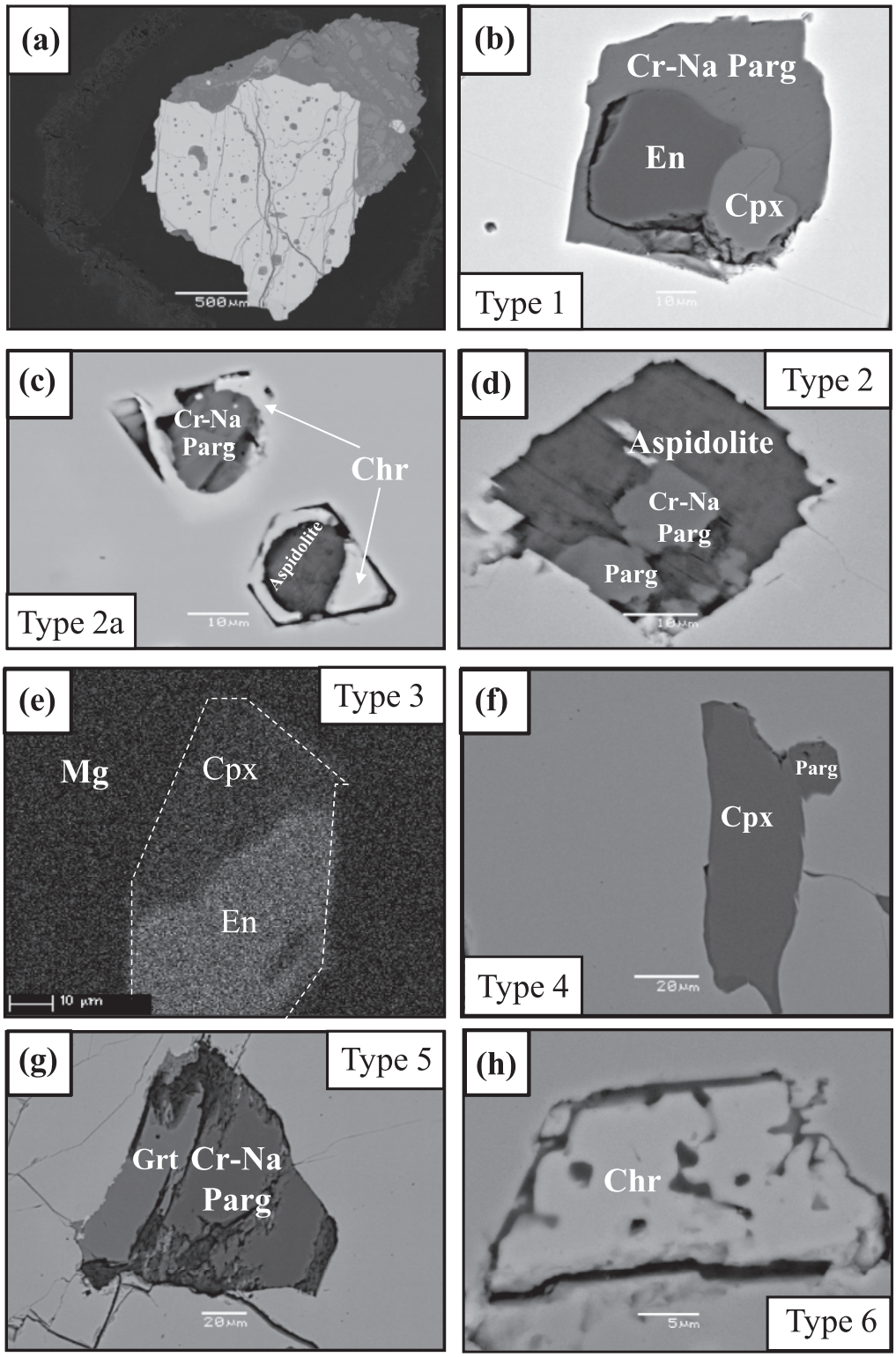

Fig. 4. Backscattered electron (BSE) images and X-ray map (using wavelength-dispersive spectroscopy; WDS) of chromite-hosted inclusions in chromitites of the Maqsad MTZ. Cr–Na Parg, Cr–Na pargasite; Aspidolite is Na phlogopite; En, enstatite; Cpx, clinopyroxene; Grt, hydrogrossular; Chr, high cr-number chromite coronas and inclusion. (a) BSE image showing the distribution of multiphase and microcrystal inclusions in the entire host chromite grain [83 OG 68(2) nodular chromitite]; (b) type 1 multiphase inclusion containing enstatite, clinopyroxene and Cr–Na pargasite [83 OG 68(2) nodular chromitite]; (c) type 2a coexisting inclusions consisting of single-phase Cr–Na pargasite and aspidolite enveloped by high cr-number chromite coronas (04 OM 31E stratiform chromitite); (d) type 2 multiphase inclusion containing Cr–Na pargasite and aspidolite [83 OG 68(1) nodular chromitite]; (e) type 3 inclusion Mg X-ray map (Kα) of enstatite and clinopyroxene [83 OG 68(2) nodular chromitite]; (f) type 4 microcrystal inclusion containing clinopyroxene and pargasite (04 OM 52D disseminated chromitite); (g) type 5 microcrystal inclusion with hydrogrossular (Grt) and Cr–Na pargasite [83 OG 68(2) nodular chromitite]; (h) type 6 microcrystal inclusion of high cr-number chromite (04 OM 52D disseminated chromitite).

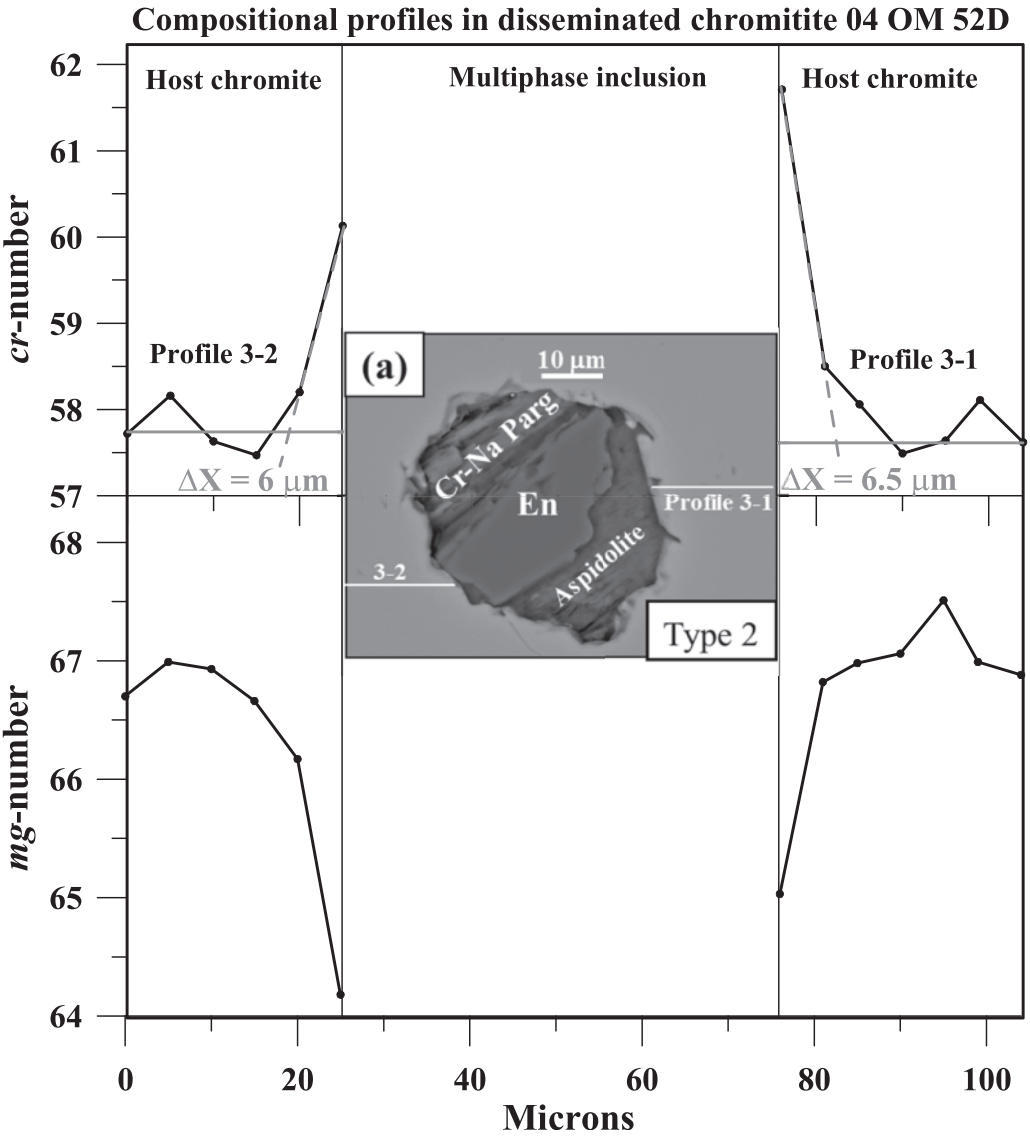

Fig. 5. (a, b) Cr-number and mg-number profiles through chromian spinel adjacent to examples of (a) type 2 and (b) 2a inclusions in the Maqsad MTZ disseminated and stratiform chromitites. ΔX is the measured length of the profile of the type 2 inclusion [see equation (1) in the main text] and is obtained by finding the intersection between the estimate of the cr-number in the core of the grain and the tangent to the concentration profile near the corona–host interface (shown by the grey lines). Data are given in Electronic Appendix. (c, d) BSE image of an example of a chromite inclusion in host chromite of the disseminated chromitite 04 OM 52D. (c) Cr-number, mg-number and (d) Fe^{2+}/Fe^{3+} in chromian spinel and melt calculated for profile A–B through the type 6 inclusion. Data are given in the Electronic Appendix. ΔX is the length measured on the profiles of type 6 inclusion [see equation (1) in the main text] and is obtained by finding the intersection between the estimate of the cr-number in the core of the grain and the tangent to the concentration profile near the inclusion–host interface (shown by the grey lines). (e) BSE image of olivine (Fo_{95}) in a type 3 inclusion overgrown by the high cr-number chromite phase (Chr) and the host chromite in the disseminated chromitite 04 OM 52D. The transition zone between the olivine grain ($Fo_{94–95}$; CaO up to 0·03 wt % and $Cr_2O_3 = 0·01$ wt % at olivine grain center) is enriched in Cr (up to $Cr_2O_3 = 0·1–0·3$ wt %) at the contact with the high cr-number chromite. Cr2O3 (wt%) and mg-number in chromian spinel (and Fo mol%, in olivine inclusion) are illustrated for profile A–B. Data are given in the Electronic Appendix. (f) BSE image of an example of altered spinel (cr-number ~30) and pargasite in a type 2a inclusion overgrown by the high cr-number chromite phase and the host chromite in the disseminated chromitite 04 OM 52D. Cr-number and mg-number in spinels are illustrated for profile A–B. Data are given in the Electronic Appendix.

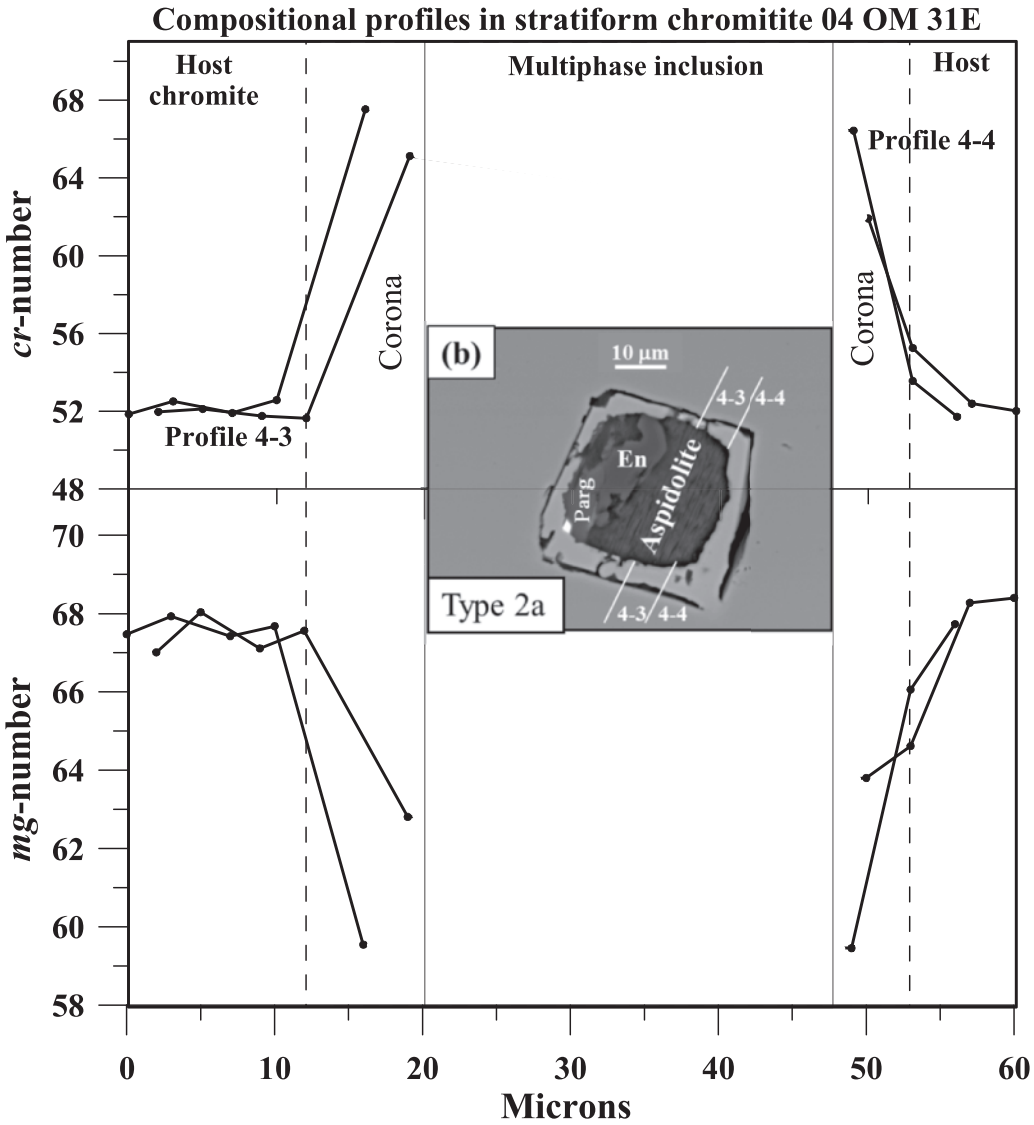

Fig. 5. (Continued)

laser fluorination for oxygen isotopes (Bindeman, 2008). Grain fractions of four chromite samples, treated in diluted HCl, rinsed with H_2O and dried, were selected for oxygen isotope analysis. To separate the primary olivine grains from the secondary serpentine, olivine fractions from three dunite samples were treated chemically at GET according to the leaching method of Snow *et al.* (1994). Three leaches were made on each crushed dunite sample, using leaching solution of 6·2 N HCl, 5% HF. The first leach was cold for 5 min, the second was in an ultrasonic bath for 10 min, and the third was in the ultrasonic bath for 10 min followed by 10 min at 125°C. The samples were then dried and the fresh olivine cores were selected for laser fluorination analysis at the University of Oregon (USA). Samples were heated with an infrared laser (9·6 μm, CO_2) in the presence of purified BrF_5 to release oxygen. The generated O_2 gas was purified in a series of cryogenic traps held at liquid nitrogen temperature, and then a mercury diffusion pump was used to remove any remaining traces of BrF_5. Oxygen was converted to CO_2 gas by reacting with graphite at high T (1450°C), the yields were measured, and CO_2 was analyzed by isotope ratio mass spectrometry (IRMS) in a dual inlet mode. Four to seven garnet standards ($\delta^{18}O = 6{\cdot}52‰$, University of Oregon garnet from Gore Mt, NY, USA named as "UOG garnet") were analyzed together with the samples during each of seven analytical sessions. Day-to-day $\delta^{18}O$ variability of standards ranged from 0·1 to 0·3‰ lighter

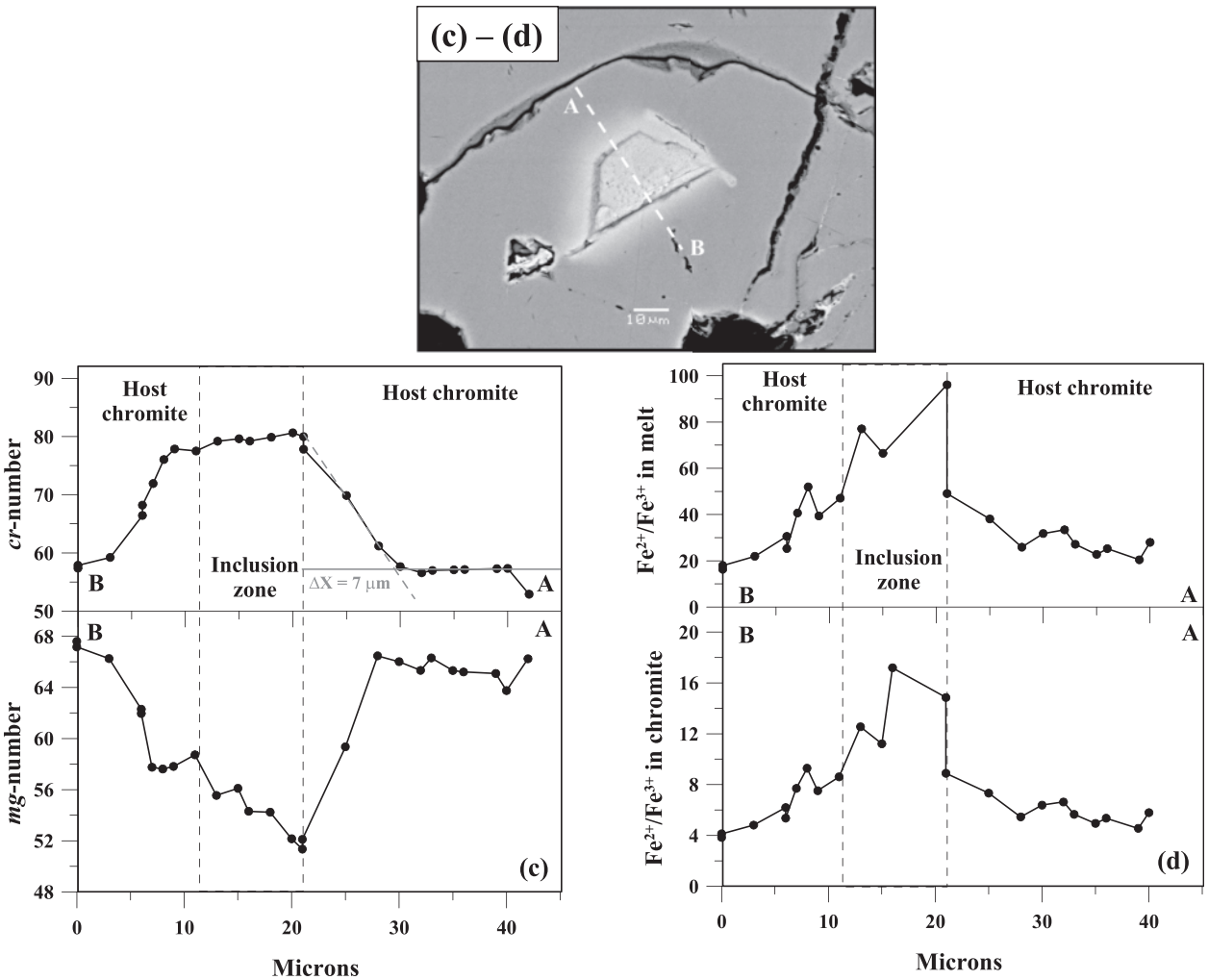

Fig. 5. (Continued)

than their reference values and the measurements of unknowns were adjusted accordingly. The precision on standards is better than 0·1‰ of 1σ standard deviation.

Homogenization experiments on selected inclusions were conducted at the University of Tasmania (Hobart, Australia) to study the silicate inclusion transformations upon heating. Hand-picked chromite grains from the nodular chromitite sample (83 OG 68-1) were placed in a platinum container and heated in a vertical furnace at 1300 ± 5°C for 3 min under high-purity argon gas flow. These conditions were found to be suitable for complete melting of the multiphase inclusions entrapped in chromite. Heating was followed by quenching in water. Then the grains were hand-picked and mounted in epoxy and polished to expose the inclusions to the surface. Silicate glasses (silicate inclusions were converted to homogeneous melt at 1300°C) in more than 60 experimentally homogenized inclusions were analysed at standard conditions (e.g. Kamenetsky *et al.*, 2001) for major elements using a Cameca SX-50 microprobe (University of Tasmania, Australia).

RESULTS

Chromite host, coronas, and inclusions

The compositions of the host chromian spinel (up to 70–80% of the chromite volume) are reported in Figs 3 and 5, Table 2, and the Electronic Appendix. The chromites in nodular sample 83 OG 68(1) have mg-numbers (54–63), cr-numbers (50–54), TiO_2 (0·6–0·9 wt %) and Fe_2O_3 (0·2–6·0 wt %) contents typical of the Maqsad MTZ nodular chromitites. Host chromian spinel in both disseminated and stratiform samples (04 OM 52D and 04 OM 31E) is also typical of the high mg-number chromites of the Maqsad MTZ. The association of chromite (cr-number = 50–62; mg-number = 54–68) with olivine ($Fo_{88–91}$) from the dunite hosting the

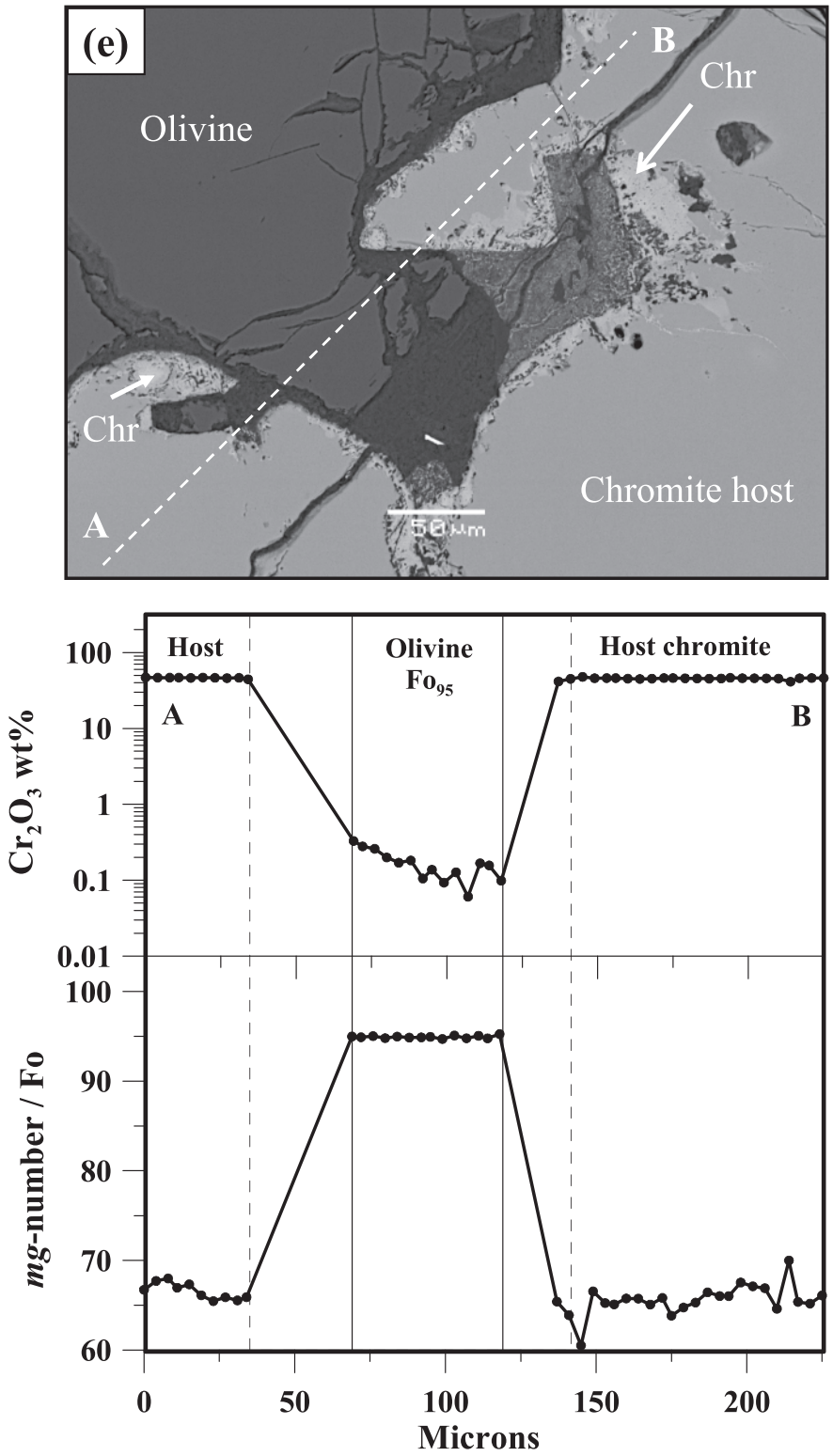

Fig. 5. (Continued)

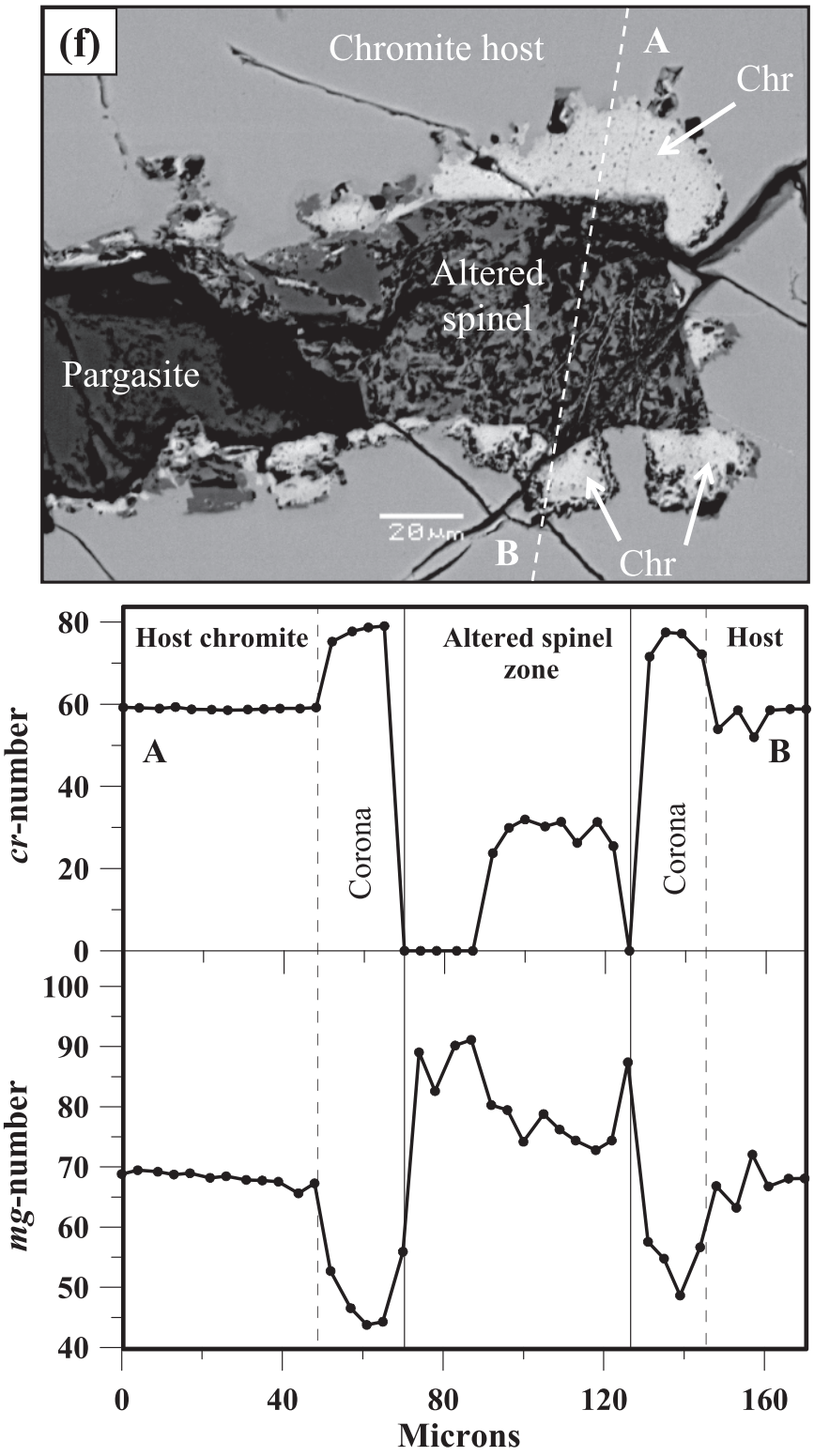

Fig. 5. (Continued)

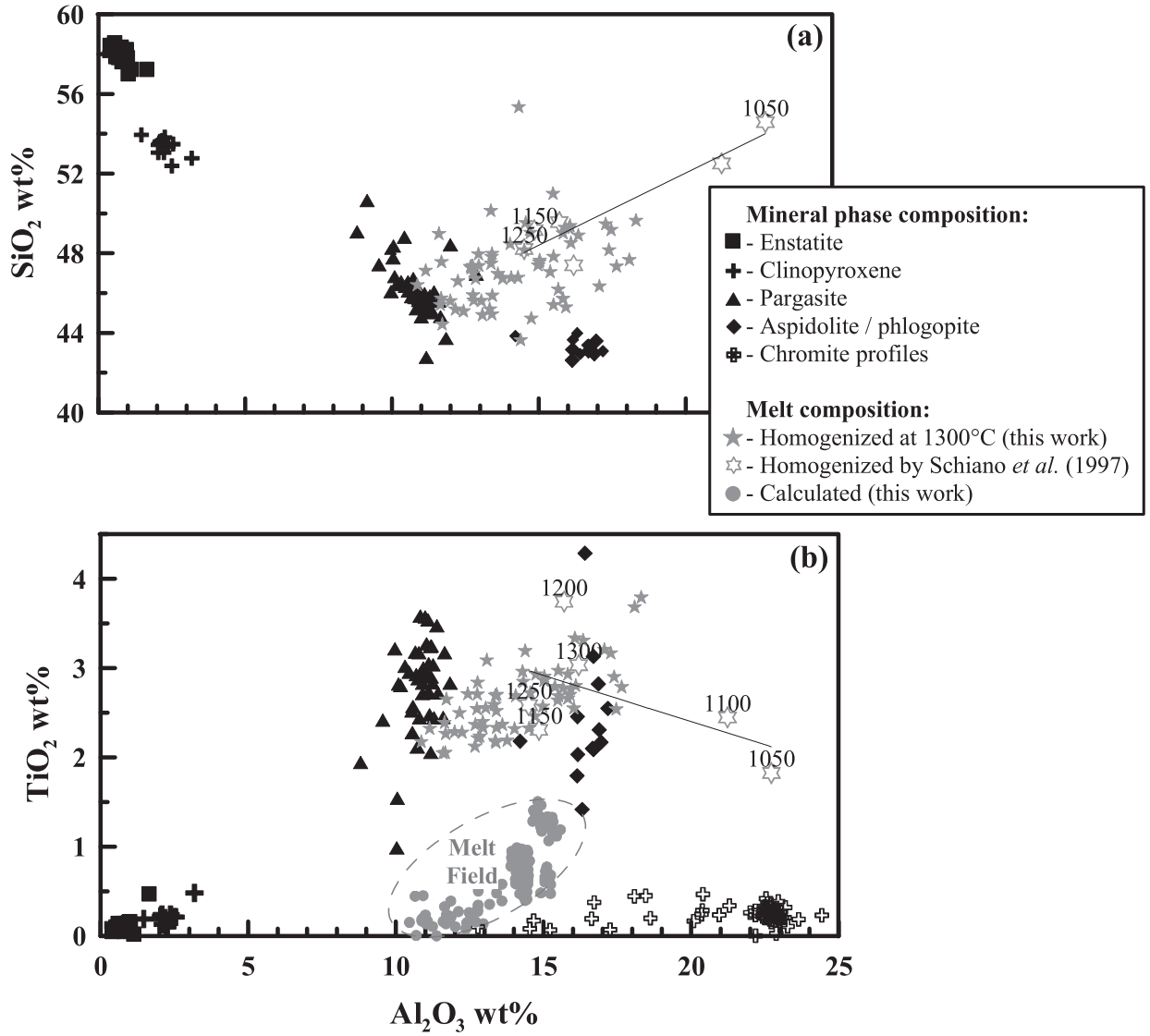

Fig. 6. (a–d) Major elements: (a) SiO_2, (b) TiO_2, (c) Cr_2O_3, (d) FeO contents vs Al_2O_3 contents in silicate and chromite phases of multiphase and microcrystal inclusions from the Maqsad MTZ nodular [83 OG 68(1,2)], disseminated (04 OM 52D) and stratiform (04 OM 31E) chromitites. Grey stars indicate the glass compositions of experimentally homogenized inclusions at 1300°C (this study). Lines show the compositional trends for melts obtained in homogenization experiments at 1050–1400°C (open stars with corresponding homogenization temperature; Schiano *et al.*, 1997). 'Chromite profiles' indicate TiO_2, FeO and Al_2O_3 contents in chromites adjacent to the multiphase inclusions. The high concentrations of FeO (up to 14 wt %) and Cr_2O_3 (1–3 wt %) in the experimentally homogenized inclusions are probably controlled by a strong diffusive Fe input from the adjacent chromite during the laboratory experiment and the initially high Cr contents in hydrous silicate minerals, respectively (see Electronic Appendix). The hydrous minerals and experimental melt compositions are recalculated on a water-free basis. In (b) the 'Melt Field' indicates the calculated TiO_2 and Al_2O_3 contents in equilibrium melts based on the compositions of the host chromite and chromite coronas and inclusions (as well as the equilibrium chromite–melt partitioning; see text). $TiO_{2\ melt}$ contents (<2 wt %) calculated based on the composition of the type 4 clinopyroxenes [and using experimental $K_d^{Cpx/melt}$ clinopyroxene–mafic melt partition coefficients from 0·27 to 0·43 of Dunn (1987), Hart & Dunn (1993) and Skulski *et al.* (1994); and $TiO_{2Cpx} = 0{\cdot}2–0{\cdot}5$ wt %] are lower than those measured in the homogenized glasses. The type 1, 2, 4 and 5 pargasite gives $TiO_{2\ melt} < 1{\cdot}2$ wt % [as calculated based on the experimental $K_d^{Amph/melt}$ amphibole–mafic melt partition coefficient range 0·95–1·29 of Adam & Green (1994) and LaTourette *et al.* (1995); and $TiO_{2Parg} = 1{\cdot}5–3{\cdot}5$ wt %], which is lower compared with the homogenized glasses. The type 2 phlogopite gives $TiO_{2\ melt} < 1{\cdot}2$ wt % [calculated based on the experimental $K_d^{Phlog/melt}$ phlogopite–mafic melt partition coefficient range 0·98–1·77 for phlogopite of Adam & Green (1994) and LaTourette *et al.* (1995); and $TiO_{2Phlog} = 1{\cdot}5–2{\cdot}5$ wt %], which is lower than that measured in the homogenized glasses. All data are given in Table 2 and the Electronic Appendix.

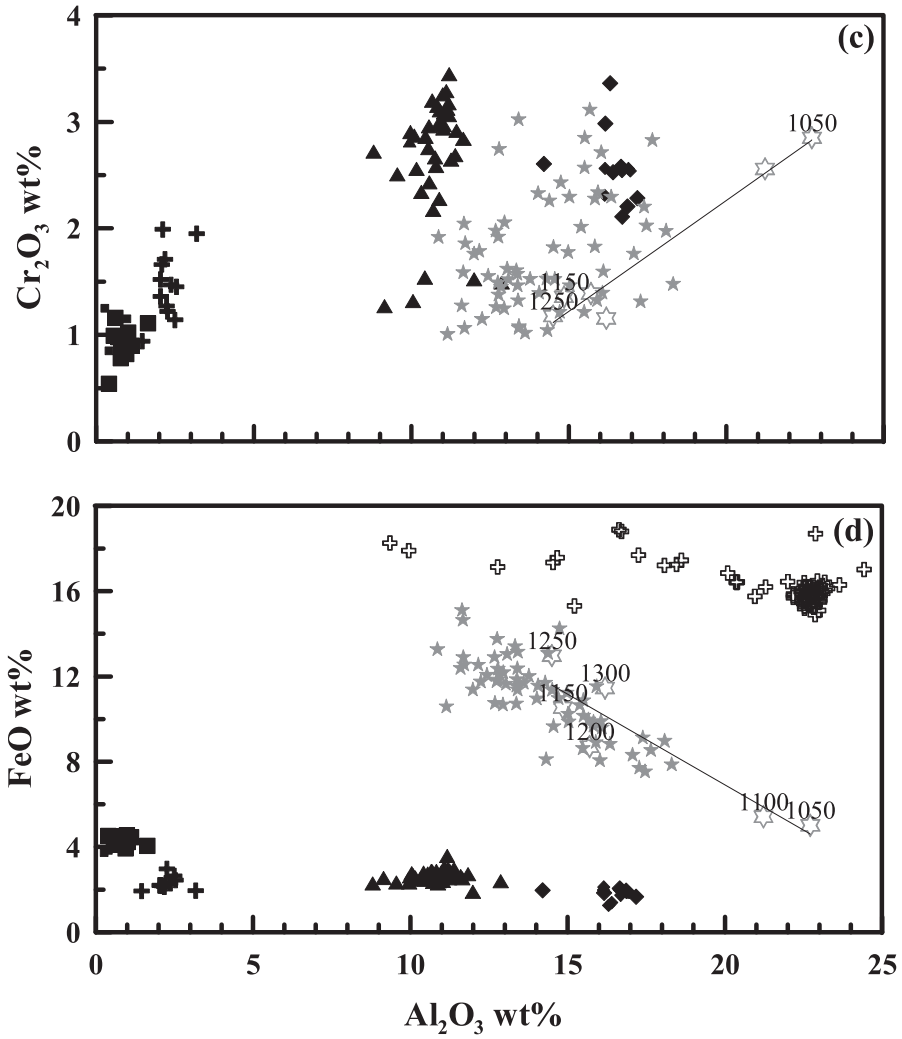

Fig. 6. (Continued)

Maqsad chromitites corresponds to the MORB field in the olivine–spinel mantle array (Arai *et al.*, 2011; and references therein). It should be noted that the mg- and cr-numbers in the host chromite of the Maqsad MTZ chromitites are typical of MORB (Fig. 3), whereas the TiO_2 and Fe_2O_3 contents plot in the intermediate field between those of the typical MORB and the hydrothermally altered harzburgites.

Typical compositional profiles through chromite coronas and inclusions (up to 10–15% of the chromite volume) are shown in Fig. 5. The chromite coronas in nodular, disseminated and stratiform chromitites have high cr-numbers (68–80) and low mg-numbers (50–58). A similar range of high cr-numbers (73–80) and low mg-numbers (54–60) is observed in the chromite inclusions (Type 6) in the host chromite of the disseminated chromitites (Table 2 and Electronic Appendix). The similar idiomorphic and compositional features of the high cr-number chromite coronas and inclusions (Figs 3–5) suggest that they were formed in a common process. High cr-numbers and low TiO_2 contents in the chromite coronas and inclusions resemble those of arc boninites (Fig. 3). In contrast, the Maqsad MTZ chromite coronas and inclusions have much lower Fe_2O_3 contents than those of chromites from typical arc boninites and MORB. The Maqsad high cr-number chromites are also different from the chromites described in 'anomalous' MORB-related plutonic rocks from Ocean Drilling Program (ODP) Holes 735B (Southwest Indian Ridge) and 895 (Hess Deep) (Arai & Takemoto, 2007; Kamenetsky & Gurenko, 2007), which have higher TiO_2 and Fe_2O_3 contents. It should be noted that the extremely low TiO_2 and Fe_2O_3 contents in the Maqsad high cr-number chromites approach those of chromites in the Haylayn hydrothermally altered harzburgites of the Oman ophiolite (Fig. 3).

Table 2: The Maqsad MTZ chromite inclusions and their host chromite compositions

Label:	04 OM 52Di-incl-3	04 OM 52Di-incl-4	04 OM 52Di-incl-5	04 OM 52Di-incl-8	04 OM 52Di-incl-15	04 OM 52Di-incl-16	04 OM 52Di-incl-18	04 OM 52Di-incl-19	04 OM 52Di-incl-20
Analysis number:	50	51	52	59	85	86	88	91	92
TiO_2	0·09	0·09	0·05	0·08	0·09	0·14	0·14	D.L.	0·13
Al_2O_3	11·29	11·52	12·22	10·26	11·78	13·50	11·59	10·82	11·56
Cr_2O_3	58·26	57·32	56·93	59·70	56·36	54·37	56·43	57·09	56·85
FeO_{tot}	17·38	17·88	17·34	17·52	18·54	18·14	18·48	17·97	18·00
MnO	0·24	0·36	0·36	0·23	0·23	0·27	0·32	0·15	0·32
MgO	11·98	11·87	12·87	10·88	11·37	11·83	11·21	11·84	11·84
NiO	0·08	0·011	D.L.	0·02	0·12	0·13	0·09	0·08	D.L.
Sum	99·51	99·34	100·33	98·71	98·61	98·66	98·53	98·69	98·86
FeO*	15·11	15·67	14·89	16·55	16·05	15·83	15·99	15·81	15·50
Fe_2O_3	2·53	2·46	2·72	1·07	2·77	2·57	2·77	2·41	2·78
Fe^{2+}/Fe^{3+}_{spinel}	6·63	7·08	6·09	—	6·45	6·84	6·42	7·30	6·20
Fe^{2+}/Fe^{3+}_{melt}	33·42	36·41	29·89	—	32·25	34·81	32·08	37·91	30·64
$Al_2O_{3\ melt}$	10·88	10·97	11·24	10·46	11·07	11·71	11·00	10·69	10·99
$TiO_{2\ melt}$	0·17	0·17	0·10	0·15	0·17	0·23	0·23	<0·03	0·22
$100\,Mg/(Mg + Fe^{2+})$	58·57	57·45	60·63	53·94	55·80	57·12	55·53	57·17	57·65
$100Cr/(Cr + Al)$	77·59	76·96	75·77	79·62	76·25	72·99	76·57	77·97	76·74

Label:	04 OM 52Di-host-1	04 OM 52Di-host-2	04 OM 52Di-host-3	04 OM 52Di-host-4	04 OM 52Di-host-5	04 OM 52Di-host-6	04 OM 52Di-host-8	04 OM 52Di-host-9	04 OM 52Di-host-10
Analysis number:	53	54	57	58	65	66	89	90	96
TiO_2	0·21	0·18	0·23	0·21	0·13	0·08	0·18	0·29	0·19
Al_2O_3	22·59	22·57	22·43	22·70	20·22	22·78	22·60	22·48	22·37
Cr_2O_3	45·68	45·46	45·64	46·13	48·62	45·06	45·14	44·63	45·11
FeO*	12·65	12·11	12·19	12·28	12·75	12·89	12·49	12·01	12·01
Fe_2O_3	2·93	3·63	3·69	3·67	3·33	3·07	3·75	3·95	3·60
MgO	14·75	15·01	15·13	15·37	14·43	14·40	11·68	15·03	15·05
Fe^{2+}/Fe^{3+}_{spinel}	4·79	3·71	3·67	3·72	4·26	4·66	3·71	3·38	3·71
Fe^{2+}/Fe^{3+}_{melt}	21·85	15·65	15·41	15·71	18·73	21·08	15·62	13·83	15·64
$100\,Mg/(Mg + Fe^{2+})$	67·52	68·84	68·86	69·06	66·86	66·57	67·83	69·04	69·08
$100Cr/(Cr + Al)$	57·58	57·47	57·73	57·70	61·74	57·03	57·27	57·13	57·50

*FeO, Fe_2O_3, Fe^{2+}/Fe^{3+} in spinel are calculated according to spinel stoichiometry; Al_2O_3 and Fe^{2+}/Fe^{3+} in melt are calculated after Maurel & Maurel (1982*a*, 1982*b*, 1982*c*). TiO_2 in melt is calculated after Kamenetsky *et al.* (2001) and Rollinson (2008) using the equation for 'Arc'. SiO_2 contents are below 0·5 wt %. D.L., values below detection limit.

Chromite-hosted inclusion types and mineral associations

The Maqsad MTZ chromite-hosted multiphase and microcrystal inclusions consist of silicate, sulphide and chromite of 1–50 μm in size. Silicates make up to 20% of the host chromite grain surface (Fig. 4a). Six main types and one sub-type of inclusion are distinguished based on inclusion shape (rounded to octahedral, anhedral to euhedral), mineral assemblages and composition; they are summarized in Table 1 and illustrated in Figs 4b–h and 5a–f.

Type 1, 2 and 2a multiphase inclusions

Type 1, 2 and 2a multiphase inclusions are composed of hydrous and anhydrous silicates and minor sulphides, and are always associated with high cr-number coronas (Table 1). Type 1 contains abundant Cr–Na pargasite, and types 2 and 2a contain aspidolite (Na phlogopite). In type

1, 2 and 2a inclusions, Cr–Na pargasite surrounds enstatite located in the inclusion core and is associated with aspidolite; it is occasionally co-entrapped with clinopyroxene (Fig. 4b–d). Subtype 2a inclusions are distinguished from the main type 2 by euhedral coronas of high cr-number chromite overgrowing pargasite, aspidolite or phlogopite (Fig. 4c). The chromite-hosted micas have variable Na_2O and K_2O contents ranging from aspidolite to phlogopite (phlogopite occurs only in the type 2a inclusions of the stratiform chromitite; Electronic Appendix). Rare inclusions of an altered spinel and serpentine assemblage are also associated with high cr-number coronas (Fig. 5f, Table 1).

Type 3, 4, 5 and 6 microcrystal inclusions

Type 3, 5 and 6 inclusions are euhedral microcrystals of silicates and high cr-number chromite. Type 3 inclusions contain an association of clinopyroxene with enstatite [limited by a single crystal in nodular chromitite, sample 83 OG 68(2); Fig. 4e] associated with the host chromite. In contrast, the high cr-number chromite phases are found adjacent to type 3 forsterite grains (Fig. 5e), suggesting that the olivine is associated with the high cr-number chromite rather than with the host chromite. In addition, type 4 anhedral inclusions associated with the host chromite contain clinopyroxene and bytownite partially transformed into secondary phases (Table 1), sometimes associated with Cr–Na pargasite (Fig. 4f). In addition, anhedral type 5 inclusions, also associated with the host chromite, are composed of hydrogarnet and occur alone or in association with Cr–Na pargasite (Fig. 4g). Type 6 inclusions are euhedral microcrystals of high cr-number chromite (Figs 4h and 5c, d). Their euhedral shape indicates a primary origin and an early entrapment into the host chromite.

Silicate mineral composition

The compositions of Cr–Na pargasite, aspidolite, phlogopite, olivine, clinopyroxene and enstatite are summarized in Fig. 6 and the complete dataset is provided in the Electronic Appendix. The composition of the chromite-hosted plagioclase (An_{86}) is in the range of that in orthopyroxene-rich, high-Mg gabbronorites depleted in incompatible trace elements drilled from the Mid-Atlantic Ridge at Deep Sea Drilling Project (DSDP) Site 334 (Nonnotte *et al.*, 2005), of those from the periphery of the Maqsad diapir (Benoit *et al.*, 1999), and of those of the Maqsad mantle plagiogranites (Amri *et al.*, 1996). In contrast, the chromite-hosted Fe–Mg silicates have higher mg-numbers (90–97) and Cr_2O_3 (0·5–4 wt %) than (1) those from the troctolitic and gabbroic cumulates, occurring in the crustal section of the Maqsad area and filling former melt channels and dykes in the Maqsad mantle diapir (e.g. Python & Ceuleneer, 2003), (2) those from the Maqsad mantle plagiogranites (Amri *et al.*, 1996), and (3) those from the DSDP Site 334 gabbronorites (Nonnotte *et al.*, 2005). The Maqsad MTZ clinopyroxenes (varying from augite to diopside in composition), Cr–Na pargasite, and micas are variable in TiO_2 (typically 0·2–0·5 wt %, 1·5–3·5 wt %, and 1·7–4·0 wt %, respectively, Fig. 6).

Composition of homogenized inclusions

The glasses obtained from the homogenization experiments at 1300 ± 5°C show large variations in the concentrations of major elements, especially Al_2O_3 (10–18 wt %), SiO_2 (44–56 wt %) and CaO (4–10 wt %) (Fig. 6; Electronic Appendix). These compositions are similar to those of 'polymineral' solid inclusions from the chromitite dyke homogenized at 1300°C by Schiano *et al.* (1997). In the latter study, the inclusions were homogenized at 1050–1400°C. They show that compositional trends in all homogenized inclusions are controlled by incongruent melting with formation of olivine at 1150–1200°C. Intra-inclusion homogeneity of the quenched glasses was observed by Schiano *et al.* (1997) only at ≥1300°C. The average TiO_{2melt}, Al_2O_{3melt}, FeO_{melt} and MgO_{melt} contents in the homogenized inclusions are 2·6 ± 0·4 wt %, 14 ± 2 wt %, 11·1 ± 1·8 wt %, and 10·5 ± 2·1 wt %, respectively, whereas the corresponding host chromite contains average TiO_{2Chr}, Al_2O_{3Chr}, FeO_{Chr} and MgO_{Chr} contents of 0·4 ± 0·05 wt %, 23 ± 1 wt %, 12 ± 0·7 wt %, and 15·4 ± 0·5 wt %, respectively (for ~60 pairs of the homogenized inclusion–host chromite, see Electronic Appendix). The corresponding partition coefficients ($K_d^{Chr/melt}$) between the host chromite and the melts homogenized at 1300°C are: $K_{d\ Ti} = 0{\cdot}15 \pm 0{\cdot}03$; $K_{d\ Al} = 1{\cdot}7 \pm 0{\cdot}2$ and $K_{d\ Fe/Mg} = (FeO_{Chr}MgO_{melt})/(FeO_{melt}MgO_{Chr}) = 0{\cdot}7 \pm 0{\cdot}1$ (see Electronic Appendix). The partition coefficient $K_d^{Chr/melt}$ for Ti is far from the equilibrium chromite–melt partitioning summarized by Kamenetsky *et al.* (2001), which is ~0·8 at $TiO_{2Chr} = 0{\cdot}4$ wt %. In contrast, Al_2O_{3melt} contents (average 14 ± 2 wt %) and FeO/MgO_{melt} ratios (average 1·1 ± 0·1) in the homogenized melts are in accord with equilibrium with the host chromite (Electronic Appendix). The high concentrations of FeO (up to 14 wt %) in the homogenized inclusions heated to 1300°C would require a strong diffusive Fe input from the chromite coronas or host during the experiment (e.g. Kamenetsky *et al.*, 2001; Danyushevsky *et al.*, 2002). The elevated Cr_2O_3 contents (average 1·8 ± 0·5 wt %) in the quenched glasses are probably due to the initial high Cr_2O_3 contents in the hydrous silicate minerals and additional chromite dissolution in the melt (e.g. Murck & Campbell, 1986).

Oxygen isotope signatures of chromites and olivines from the Maqsad MTZ

We performed the first measurements of the oxygen isotope composition of chromite and associated olivine grains in the MTZ of the Oman ophiolite. The $\delta^{18}O$ values of

chromite grains (Maqsad chromitites) vary from 3·2 to 3·7‰ (Table 4). The $\delta^{18}O$ values of single olivine grains in the associated Maqsad dunites vary from 5·2 to 5·8‰, which is similar to and slightly higher than the 5·18 ± 0·28‰ reported for olivines from mantle peridotites (Mattey *et al.*, 1994), perhaps reflecting protolith seawater alteration at low temperatures.

DISCUSSION

Was a silicate melt involved in the Maqsad Moho Transition Zone petrogenesis?

In this section we use the composition of the Maqsad MTZ chromites, together with the new data from this study and published experiments on the homogenization of the chromite-hosted multiphase inclusions, to better constrain the origin of the chromite-hosted inclusions. The known sensitivity of the Cr/Al ratio in chromian spinel to water activity and the composition of the original melt (Irvine, 1975; Onuma & Tohara, 1981; Dick & Bullen, 1984; Roeder & Reynolds, 1991) can be used to better constrain these parameters during chromite crystallization. Calculations of the melt composition using the analysed chromite compositions and reported experimental chromite–melt partitioning coefficients (Maurel & Maurel, 1982*a*, 1982*b*, 1982*c*; Kamenetsky *et al.*, 2001; see Table 2 and Electronic Appendix) imply that the melts in equilibrium with the host chromite of the nodular, disseminated, and stratiform chromitites had high $Al_2O_{3\ melt}$ (~14·5 wt % on average) and $TiO_{2\ melt}$ (0·8 wt %) contents, FeO/MgO_{melt} of ~1, and high mg-numbers (~65), consistent with primitive tholeiitic MORB-like compositions (Fig. 6b; Electronic Appendix). The calculated melts in equilibrium with the high cr-number chromite coronas and inclusions had lower $Al_2O_{3\ melt}$ (10–11 wt %) and $TiO_{2\ melt}$ (≤0·3 wt %) contents, but similar mg-numbers of ~65 (Table 2). The $TiO_{2\ melt}$ contents are much lower than those measured in the homogenized glasses (2–4 wt %, Fig. 6b). Moreover, the temperature stability domain of amphibole and micas and associated chromites below 1050°C (see discussion below; Table 3) indicates that the observed homogenization temperature of 1300°C for the multiphase inclusions is much higher than the true temperature of the Maqsad MTZ chromitite crystallization. Therefore, neither host chromite, high cr-number inclusions and coronas, nor silicate minerals in the multiphase inclusions could have crystallized from the experimentally produced melts. The large inter-inclusion compositional variation of the melts can be explained only by heterogeneous entrapment of silicates (i.e. variable proportions of enstatite, pargasite, aspidolite and/or phlogopite). The euhedral shapes of the high cr-number coronas and inclusions and their predominance over the silicate phase in the multiphase inclusions (Figs 4c and 5b) indicate that the high cr-number chromite crystallized early, either as microcrystals (Figs 4h and 5c, d) or as chromite overgrowths on the silicate crystals or their assemblages (Fig. 5e and f) rather than as a daughter phase from the homogenized melt as previously suggested by Schiano *et al.* (1997) and Borisova *et al.* (2008).

In the framework of an entirely magmatic scenario, non-equilibrium (fractional) crystallization of the host chromite accounts for the preservation of early-stage phases (high cr-number chromite). However, our homogenization experiments provide no evidence either for entrapment of a melt phase or for a melt–crystal reaction (e.g. incongruent reaction with melt formation), which could be responsible for the Maqsad chromite crystallization. We did not find any geological evidence for a close association of the Maqsad chromitites with pyroxenites or anorthosites. Therefore, a chromitite origin by incongruent dissolution of pyroxene or feldspar into an olivine + chromite-saturated melt (Bédard & Hébert, 1998; Bédard *et al.*, 2000) is also unlikely for the Maqsad MTZ chromitites. Because the experimentally homogenized melts are well explained by heterogeneous trapping of silicates, the Maqsad MTZ chromites could not have crystallized from an arc boninite melt, in contrast to the suggestion of Schiano *et al.* (1997).

Constraints on T–P–α_{H2O} conditions of the Maqsad MTZ chromitite crystallization

The mineral assemblages of the chromite-hosted inclusions, together with available experimental and geological data on mineral phase equilibrium, provide new constraints on the chromite crystallization sequence and the T–P–α_{H2O} conditions during chromitite crystallization (Table 3).

High cr-number chromite corona and inclusion crystallization

The first group of constraints stems from the multiphase inclusions (Types 1, 2 and 2a) and euhedral type 3 inclusions associated with the high cr-number chromite coronas. The high mg-numbers of the chromite-hosted Fe–Mg silicates are consistent with high water activity ($\alpha_{H2O} = 1$) in the crystallizing melt (e.g. Koepke *et al.*, 2009) or its crystallization directly from a high-temperature aqueous fluid (e.g. Python *et al.*, 2007). Phase-equilibria experiments (e.g. Presnall, 1995; Feig *et al.*, 2006) indicate that, in the presence of an H_2O or H_2O–CO_2 phase, pargasitic amphibole forms from a silicate melt or fluid between 700 and 1000°C and $P \geq 50$ MPa. Above 900–1000°C, chromian pargasite transforms into olivine, chromite and a melt (Johan & Le Bel, 1978), although pargasite may be stable at higher T in the presence of high F and Cl contents (e.g. Presnall, 1995). It is well known that a miscibility gap exists in the aspidolite–phlogopite solid solution at 200 MPa and 700°C (e.g. Costa *et al.*, 2001, and references therein). Thus, where aspidolite (Na end-member),

Table 3: T–P–f_{O2} conditions and model stages responsible for the Maqsad MTZ chromitite petrogenesis

Model stages:	Serpentinized mantle protolith	Prograde metamorphism	Assimilation by MORB
Stage number:	I	II	III
Altered spinel	+	−	−
Serpentine assemblage	+	−	−
High cr-number chromite	−	+	−
Forsterite	−	+	−
Phlogopite	−	+	−
Aspidolite	−	+	−
Clinopyroxene	−	+	+
Enstatite*	−	+	+
Cr–Na pargasite	−	+	+
Plagioclase	−	−	+
Host chromite	−	−	+
Inclusion types:	2a	1, 2, 2a, 3, 6	4, 5
Pressure† (MPa):	200?	200	200
Temperature† (°C):	≤600	600–950 (±10)	950–1050 (±10)
Redox conditions‡ (log f_{O2}, bars)	—	−14 to −12	-11
Oxygen buffer:	—	QFM – 2·7 to QFM at 600–950°C	QFM – 0·4 at 1000 ± 15°C
Olivine–chromite assemblage‡	—	The Maqsad MTZ type 3 inclusion (Fo_{95-96}) and incongruent olivine (Fo_{85-91})§ + High cr-number chromite coronas and inclusions	Olivine (Fo_{88-91}) from the Maqsad MTZ dunites + Host chromite from the Maqsad MTZ chromitites

*Rare presence of enstatite in chromitite matrix.
†Temperatures were estimated based on the available experimental data on silicate mineral phase equilibrium (see text). The pressure of 200 MPa used for the calculation (see below) is based on the thickness of the geological sequence of the Maqsad area (see text).
‡Oxygen fugacity and closure temperature for the olivine–chromite assemblages were calculated following O'Neill & Wall (1987) and Ballhaus *et al*. (1991) at 200 MPa. The log units of fO_2 are relative to the quartz–fayalite–magnetite (QFM) oxygen buffer.
§Composition of incongruent olivine appearing during homogenization experiment on polymineralic inclusions is after Schiano *et al*. (1997).
Composition of olivine Fo_{88-91} from the Maqsad MTZ dunites, which are the host rocks for the investigated MTZ chromitites, is according to Abily & Ceuleneer (in press).
+ indicates presence of the phase or assemblage.

phlogopite (K end-member) and Cr–Na pargasite are all present in type 2a chromite-hosted inclusions (Figs 4c and 5b), all phases could have crystallized from a hydrothermal fluid at temperatures as low as 700°C and pressures of 200 MPa. The association of clinopyroxene with enstatite and pargasite found in one inclusion of type 1 (Fig. 4b) and in type 3 (Fig. 4e) suggests that these phases crystallized simultaneously and were entrapped near the two-pyroxene closure temperature of 860–900°C (obtained according to Wells, 1977). It should be noted that the Maqsad MTZ chromite-hosted Cr–Na pargasite and aspidolite contain high Na_2O and Cl concentrations reaching 6 and 0·4 wt %, respectively. Therefore, the assemblage of type 1–3 inclusions with high cr-number

Table 4: Oxygen isotope composition $\delta^{18}O$ (‰) of the Maqsad MTZ chromitites and host dunites

Host dunites	Olivines*	Chromitites	Chromites
11 TUF1	5·8 ± 0·1	83 0G 68 (1)	3·2 ± 0·1
11 TUF2	5·4 ± 0·1	83 0G 68 (2)	3·8 ± 0·1
11 TUF7	5·2 ± 0·1	04 OM 52D	3·6 ± 0·1
		04 OM 31E	3·5 ± 0·1

*Oxygen isotope composition of the mineral fractions measured at the University of Oregon (USA).

chromite (Tables 1 and 3) may have crystallized in the presence of an aqueous NaCl-bearing fluid. Our estimates of closure temperature for olivine inclusions and high cr-number chromite fix the lowest temperature of the high cr-number chromite crystallization at 600–630°C [obtained using equations of O'Neill & Wall (1987) and Ballhaus *et al.* (1990, 1991) at 200 MPa, Table 3]. Thus, a T of 600–950°C and P of ~200 MPa for high cr-number chromite crystallization corresponds to subsolidus conditions for a hydrous mafic melt (similar to primitive MORB; Feig *et al.*, 2006) and implies metamorphic recrystallization in the presence of an NaCl-bearing fluid.

Host chromite crystallization

The second group of constraints stems from anhedral type 4 and 5 inclusions. The ore bodies were emplaced and crystallized at the base of the oceanic crust whose stratigraphic thickness does not exceed 6 km. This places a major geological constraint for the maximum lithostatic pressure of crystallization of 200 MPa. Moreover, there is abundant crystallization of MORB-type tholeiites along the low-pressure olivine–plagioclase cotectic (troctolitic cumulates) evolving to the olivine–plagioclase–clinopyroxene cotectic as temperature decreases (olivine gabbro cumulates) in impregnations, sills, and dykes adjacent to the chromitite ore bodies (Korenaga & Kelemen, 1997, and references therein). This provides further evidence for low-pressure conditions in the Maqsad MTZ. Type 4 and 5 inclusions, containing plagioclase (An_{86}) in association with anhedral pargasite (Fig. 4f and g), could be at equilibrium at 800–1120°C and 200–300 MPa according to the geothermometer of Holland & Blundy (1994). To avoid complete destabilization of the chromite-hosted pargasite, the chromite crystallization should occur in the pargasite stability field (below 1070°C; Muntener *et al.*, 2001). Indeed, Feig *et al.* (2006) demonstrated that H_2O-saturated MORB melts crystallize pargasite below 1020°C in equilibrium with chromite at pressures of ~500 MPa. Thus, our findings of the same assemblage of chromite with pargasite, clinopyroxene and plagioclase at lower pressures (200 MPa) in the Maqsad MTZ offer two possibilities: (1) pargasite crystallization from a fluid-saturated (~5 wt % H_2O at ~200 MPa) mafic melt ('magmatic' scenario), or (2) direct pargasite precipitation from an aqueous fluid or recrystallization from another silicate mineral in the presence of fluid ('subsolidus scenario'). We prefer the first hypothesis for the host chromite crystallization because, in the case of a water-saturated MORB system at 200 MPa, hydrous MORB melt is present above 950°C (Berndt *et al.*, 2005; Feig *et al.*, 2006), and the host chromite shows compositions similar to MORB chromites (Fig. 3). However, the second 'subsolidus scenario' cannot be completely excluded. Thus, the host chromite may crystallize at 950–1050°C from a water-saturated hybrid MORB melt (see discussion below). Therefore, P of 200 ± 50 MPa and T from 600 to 1050°C are likely to be the range of conditions of the Maqsad MTZ chromite formation in a water-bearing system.

Constraints on redox conditions and mantle source

The major challenge in understanding chromitite formation is to identify a mechanism that concentrates Cr given that it has a low solubility in basaltic melts (Roeder & Reynolds, 1991) and aqueous fluids at redox conditions corresponding to the quartz–fayalite–magnetite buffer (QFM) (see below). Our data suggest that the Maqsad MTZ chromitites crystallized in the presence of an aqueous fluid and/or a hydrous melt sharing many characteristics with MORB. Because MORB magmas are generally dry (e.g. Danyushevsky *et al.*, 1996; Asimov & Langmuir, 2003), these conditions require an external source of water. The strong decrease in Fe^{2+}/Fe^{3+} in the profiles from chromite inclusions to the host chromite (Fig. 5d) indicates a sharp change in temperature and/or oxygen fugacity upon the chromite crystallization [f_{O2} is calculated based on the olivine–chromite equilibrium of O'Neill & Wall (1987) and Ballhaus *et al.* (1990, 1991) at 200 MPa, Table 3]. Initially high Fe^{2+}/Fe^{3+} ratios (up to ~16) are similar to those of chromite from the Oman metamorphic harzburgites (Fe^{2+}/Fe^{3+} = 12–16), whereas Fe^{2+}/Fe^{3+} values of 3–5 are typical magmatic values (e.g. Kamenetsky *et al.*, 2001). Three independent arguments provide evidence for reducing conditions during the early stages of the chromite crystallization in the presence of a high-temperature fluid: (1) extremely high Fe^{2+}/Fe^{3+} ratios in early (high cr-number) chromite (Table 2, Fig. 5d); (2) elevated Cr contents (probably in the form of Cr^{2+}) in the silicate-phase inclusions (Fig. 6); (3) low oxygen fugacity inferred from the olivine–chromite equilibrium. The reducing conditions (from QFM − 2·7 to QFM at 600–1000°C, Table 3) evidenced for the chromite crystallization strongly support the derivation of the chromite grains from serpentinized oceanic lithospheric mantle rather than from more oxidized fluids from the subducting slab, at least in the Maqsad area of the Oman ophiolite. Only serpentinized oceanic mantle can provide highly reducing fluids as evidenced by native iron in the serpentinized peridotites from the Maqsad area (Lorand, 1987). Methane-rich fluids are observed as olivine-hosted inclusions in hydrated harzburgite (Sachan *et al.*, 2007). The initial stages of dehydration of methane-bearing serpentinized mantle could result in the liberation of such aqueous CH_4-bearing fluids. Highly reduced C–O–H fluids have been documented in chromite-hosted inclusions in the Kempirsai ophiolites from the mantle–crust transition zone (Melcher *et al.*, 1997), and highly reducing conditions have also been inferred for the Thetford Mines ophiolite (Pagé *et al.*, 2008). Our estimates of the redox conditions of the chromite-hosted fluid, based on the

Kempirsai fluid inclusion data (Melcher *et al.*, 1997) using the SUPCRT thermodynamic database (Sverjensky *et al.*, 1997), yield oxygen fugacity between QFM − 5 and QFM − 2 at 1000°C and 200 MPa. The Cr_2O_3 (0·8–2·0 wt %) and 100 Mg/(Mg + Fe^{2+}) (92–96) values in the Maqsad MTZ type 2 and 3 pyroxenes and forsterite inclusions are much higher than those typical of the Maqsad harzburgites (≤0·8 wt % and ~91, respectively; G. Ceuleneer, unpublished data), suggesting that these phases are not xenocrysts derived from water-poor harzburgitic mantle. The Maqsad MTZ assemblage of high cr-number chromite (low Fe_2O_3) with forsterite ($Fo_{95–96}$), pyroxene (mg-number = 92–94), and pargasite (mg-number = 90–94) inclusions (Tables 2 and 3; Electronic Appendix) suggests their origin to be from a highly refractory mantle source, probably hydrated harzburgite.

Constraints on Cr mobility in high-temperature fluids

The hydrous silicates of the chromite-hosted inclusions are either magmatic or high-temperature hydrothermal phases as indicated by their high TiO_2 (≥0·5 wt %) and Cr_2O_3 (≥1·5 wt %) concentrations, because both Ti^{4+} and Cr^{3+} are generally not mobile in low- to moderate-temperature aqueous fluids (≤450°C; e.g. Crerar *et al.*, 1985). In addition, high T and reducing conditions favour lower oxidation states of multivalent elements (Fe and Cr), which are far more soluble. Thus, the high Cr content (up to 4 wt % Cr_2O_3) in the Maqsad MTZ chromite-hosted silicates (Fig. 6c) might be due to abundant Cr^{2+} in the fluid–melt system. By analogy with Fe^{2+}, Cr^{2+} and its Cl complexes are expected to be far more soluble than Cr^{3+} species (e.g. Crerar *et al.*, 1985; Pokrovski *et al.*, 2003). Equilibrium calculations using thermodynamic data for Cr hydroxide complexes from the SUPCRT database (Shock *et al.*, 1997, http://geopig.asu.edu/index.html#) also indicate that the stability field of Cr^{2+} species in aqueous solution under the redox conditions of the QFM buffer widens with increasing temperature. The elevated Cr/Al ratios in boninitic melts and hydrothermal fluids may thus reflect high concentrations of Cr^{2+} in the form of chloride complexes in aqueous fluid under reducing conditions that significantly enhance the solubility of Cr^{3+}-bearing minerals, whereas the solubility of Al^{3+}- and Ti^{4+}-bearing solid phases is unaffected by the redox potential. In addition, dissolved silica may also influence Cr–Al–Ti fractionation during fluid–rock interaction. The high silica contents, evident from silicate inclusions, may promote formation of soluble metal–silicate complexes as demonstrated by experimental studies for Al, Ti and similar metals (Fe, Ga) both in moderate T–P hydrothermal solutions (Pokrovski *et al.*, 2002; and references therein) and in high T–P subduction-zone fluids (Manning *et al.*, 2008; and references therein). Such complexes may significantly enhance Cr transport by hydrothermal fluids. Such fluids may be responsible for the metamorphic recrystallization at subsolidus conditions of mineral phases rich in Cr.

An alternative or additional form of chromium transport and accumulation at subsolidus conditions may be so-called 'crystallosols' containing finely crystallized chromian spinel (Pushkarev *et al.*, 2007). The discovery in our work of micrometre-size multiphase silicates and associated high cr-number chromites in the Maqsad chromitites may represent such micron-size 'crystallosols'. This substance, when assimilated by the oxidized MORB melt, may trigger the host chromite crystallization.

Constraints on the Maqsad chromitite cooling rate from elemental diffusion profiles

The Maqsad MTZ chromite-hosted Fe–Mg silicates (forsterite, pyroxene, amphibole and mica) of type 1–5 inclusions with elevated mg-numbers (90–97) have high MgO (≥16 wt %) and low FeO (≤5 wt %) contents (Fig. 6d, Electronic Appendix) compared with the lower MgO (12–15 wt %) and higher FeO (15–20 wt %) of the host chromites. This was previously explained by subsolidus Fe–Mg exchange between the Fe–Mg silicates and host chromite (e.g. silicate enrichment in Mg and depletion in Fe after entrapment owing to diffusive re-equilibration; Johan & Le Bel, 1978; Johan *et al.*, 1983). However, this is unlikely for the following reasons: (1) the profiles through the host-chromites to silicate inclusions show no evidence for Fe–Mg exchange between the chromite and silicates (e.g. no forsterite content variation is observed in the >100 μm olivine associated with high cr-number chromite and host chromite, Fig. 5e); (2) the cooling rates (see below) are fast enough to inhibit diffusion across the silicate–chromite interface; (3) the Fe–Mg silicate mineral compositions do not show any dependence on the inclusion size (e.g. all silicates are systematically and homogeneously depleted in FeO, which is below 5 wt %; Fig. 6d). All these observations suggest originally high MgO and low FeO contents and high mg-numbers in the Maqsad MTZ chromite-hosted silicates.

We estimated closure temperatures for diffusive Fe–Mg exchange between the Maqsad MTZ host chromite and the Maqsad MTZ olivine of the host dunite to be 1000 ± 15°C at 200 MPa (see Table 3). This is much higher than the closure temperature of 681 ± 44°C proposed for slowly cooling ophiolitic peridotites (Kamenetsky *et al.*, 2001). The chromitite cooling rates may be estimated from the elemental profiles through the chromite-hosted inclusions (Fig. 5) using the diffusion models of Ganguly *et al.* (1994) and Béjina *et al.* (2009). The available data on Cr diffusion in magnesiochromite (Suzuki *et al.*, 2008; and references therein) were used to estimate the cooling rate (s)

from Cr concentration profiles using the following equation (Ganguly *et al.*, 1994; Béjina *et al.*, 2009):

$$s = 4[D_{(To)}RT_o^2]/(Ex_c^2) \quad (1)$$

where $D_{(To)}$ is the Cr diffusion coefficient in magnesiochromite ($cm^2\ s^{-1}$) at T_o, $x_c = 2(Dt)^{0.5} = 0{\cdot}564\Delta X$, where ΔX is measured on the profiles of type 2 and 6 inclusions (Fig. 5a, c) and x_c is the characteristic distance (μm) of diffusion, R is the ideal gas constant (8·3144 J $mol^{-1}\ K^{-1}$), T_o is the maximum temperature of crystallization (1273–1323 K), and E is the activation energy (J mol^{-1}) of Cr diffusion in magnesiochromite ($cm^2\ s^{-1}$). In equation (1), x_c is the only parameter that is extracted from the concentration profiles. On all the Cr concentration profiles analysed, we found x_c to be between 4 and 10 μm. Using these values, equation (1) gives a rough estimate for s between 0·003 and 0·2°C a^{-1}. The uncertainties of the estimations have been discussed by Béjina *et al.* (2009). A more precise determination of s would require the use of a multicomponent diffusion approach, but diffusion coefficients of most elements in chromites are lacking at present. Our calculated values approach the highest values reported for mid-ocean ridge crust (~0·01 °C a^{-1}, Schmitt *et al.*, 2011). Moreover, our values are close to the highest values reported for the Oman lower oceanic crust (~1°C a^{-1}, VanTongeren *et al.*, 2008). The high cooling rates inferred in our study strongly support the involvement of an aqueous fluid that was cooler than the chromite-bearing system. The preservation of both the Maqsad chromitite textures (e.g. Leblanc & Ceuleneer, 1992) and the sharp zonation of the Maqsad chromite grains provides a further support for rapid cooling in the MTZ. The fast cooling rates can be explained by active hydrothermal circulation at the Moho level of the oceanic lithosphere.

Moho Transition Zone chromitite petrogenesis: 'magmatic' versus 'subsolidus' model

To unravel the complexity of the MTZ chromitite petrogenesis and the role of differentiation processes we discuss below all the new data obtained in this study in the light of existing models of chromitite origin in ophiolite massifs.

'Magmatic' versus 'subsolidus' scenarios

Two main types of petrogenetic model for chromitite petrogenesis exist. The most popular 'magmatic' model suggests massive chromite crystallization from chromite-saturated magmas (e.g. Augé, 1987). This and similar models require oversaturation in chromium in a hydrous silicate melt owing to a sharp temperature drop or oxidation of the magmatic system in 'minichambers' (Lago *et al.*, 1982) or crustal assimilation by the olivine-saturated melt (Irvine, 1975). Entrapment of silicate melt into chromite is advocated by all these models (Lorand & Ceuleneer, 1989; Leblanc & Ceuleneer, 1992; Schiano *et al.*, 1997). We found two types of evidence for the possible presence of a melt in our system. (1) The host chromite composition is consistent with its crystallization from a MORB melt. (2) The type 4 and 5 plagioclase–pargasite inclusions are in an assemblage with the host chromite and were formed at temperatures within the stability domain of hydrous MORB melts (950–1050°C at 200 MPa, Table 3). The inclusions were possibly entrapped in the host chromite during magmatic crystallization (in case of water-saturated MORB melt at 200 MPa, Feig *et al.*, 2006). Far above 1100°C, an efficient process of re-equilibration of the high cr-number chromite with the residual melt may occur by cationic diffusion (Scowen *et al.*, 1991). However, the maximum temperature of 1050°C (Table 3) estimated here makes such a process for spinel–melt re-equilibration inefficient. In fact, the preservation of high cr-number chromite inclusions indicates extremely sluggish rates of spinel dissolution (Brearley & Scarfe, 1986) and the lack of equilibration in a mafic melt owing to fast cooling and efficient fractional separation of chromite. The fast cooling inferred in this study helps to explain the preservation of the chromite-hosted hydrous silicates (phlogopite, aspidolite, pargasite). However, the Maqsad chromite-hosted inclusions themselves provide evidence for subsolidus conditions rather than for a molten or partially molten system, which would support the second group of models discussed below.

The second group of models suggests chromite crystallization at subsolidus conditions based on the stability field of the pargasite inclusions, which is below 1070°C (e.g. Muntener *et al.*, 2001). These models state that 'the presence of sodium-rich hydrous phases indicates a high Na activity in the system and implies a temperature limit corresponding to the maximum thermal stability of pargasite' (Augé & Johan, 1988). Our investigation of the Maqsad chromitite inclusions provides several lines of evidence in favour of such subsolidus petrogenesis (below 950°C). (1) In our case we have no evidence for a silicate melt in the chromitite system, as the multiphase inclusions are low-temperature silicates heterogeneously entrapped by the growing chromite rather than crystallized as daughter phases from an entrapped melt. (2) Because 'coronas' are typical textures of 'metamorphic crystallization' and rarely for magmatic systems (Deer *et al.*, 1997), the presence of high cr-number chromite crystallized below 950°C probably indicates an early metamorphic stage of the chromite growth. (3) It helps explain the very good preservation of an association of hydrous minerals such as aspidolite and phlogopite (which are not stable above 700°C) and pargasite (which is not stable above 1050°C). Such preservation of multiphase inclusions would indicate subsolidus rather than magmatic conditions to avoid the complete destabilization and/or melting of entrapped in

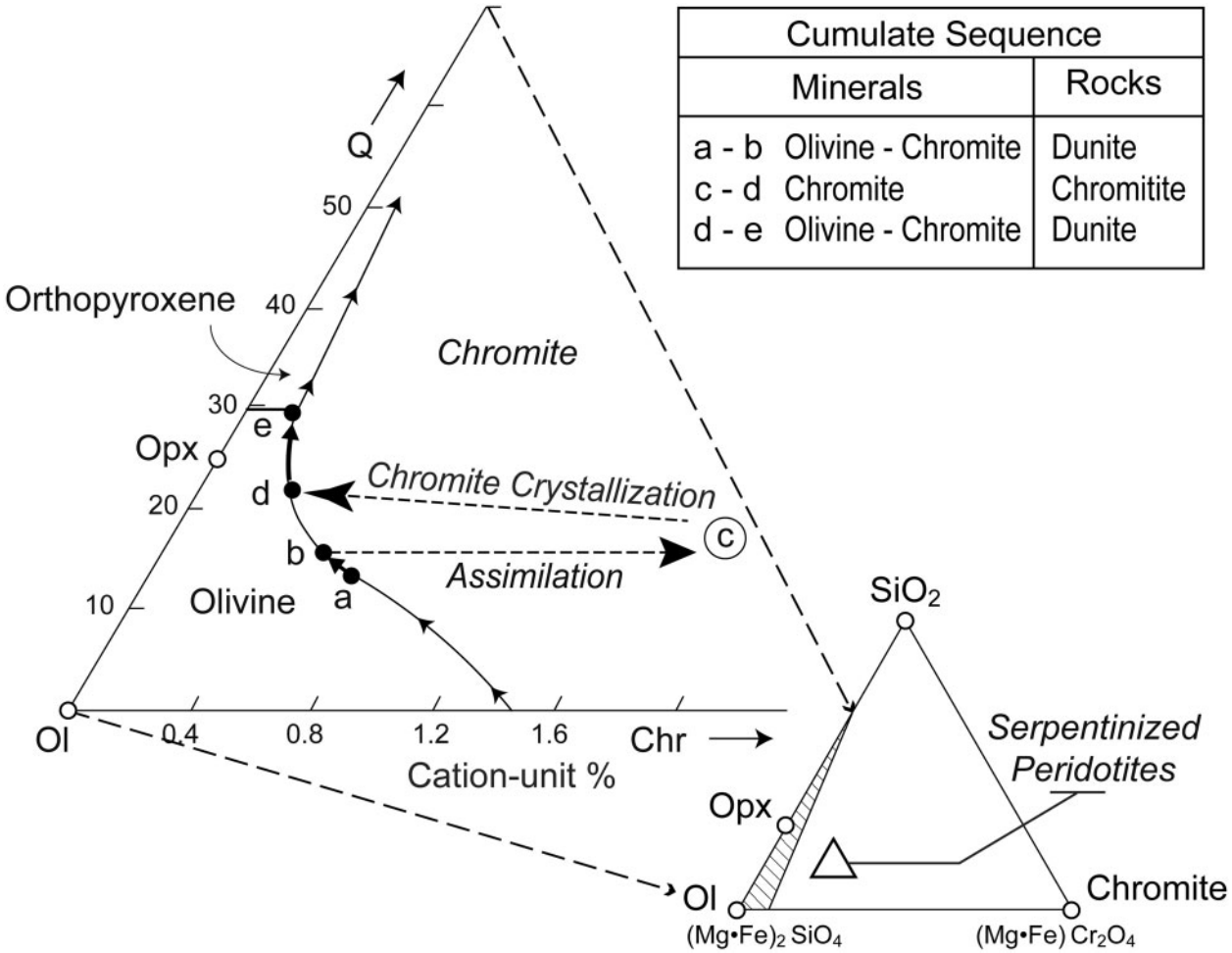

Fig. 7. Phase diagram model of Irvine (1975) applied to the petrogenetic model of the Maqsad MTZ chromitites formed through assimilation of a metamorphic mantle protolith by olivine-saturated MORB and fractional crystallization. The assimilation (b–c) is shown as a distinct process from the crystallization (a–b, c–d, and d–e). In reality, however, chromite could crystallize while the metamorphic protolith was being continuously assimilated. The composition of the serpentinized harzburgites corresponds to those of Li & Lee (2006).

chromite aspidolite and pargasite phases. Figure 5e and f demonstrates textural relationships between silicate phases, high cr-number and host chromites that are not typical for magmatic systems. It can be seen that the high-Mg silicate and altered spinel phases were overgrown by high cr-number chromites similar to some hydrothermal or metamorphic systems.

Three-stage model for the Maqsad MTZ chromitite petrogenesis

Some of our data are consistent with the magmatic processes, whereas others support the subsolidus models described above. We believe that both types of model can be reconciled within a single scenario involving three stages: (1) retrograde metamorphism (serpentinization) of a mantle protolith that was the primary source of chromium and water; (2) prograde metamorphism of this serpentinized protolith (or serpentinite dehydration); (3) magmatic assimilation by MORB (Table 3; Figs 7 and 8).

Although the first stage is generally poorly preserved, it is evidenced by rare inclusions of serpentine and altered spinel in stratiform and disseminated chromitites (Fig. 5f; Tables 1 and 3), which are typical of serpentinized peridotites formed by hydration of the upper mantle at $\leq 600^{\circ}$C (e.g. Li & Lee, 2006). Moreover, serpentinites and serpentinized harzburgites are enriched in chromium with concentrations higher than 3000 ppm Cr (Li & Lee, 2006) and, therefore, may constitute an abundant chromium source. Thus, deep harzburgites serpentinized as a result of interaction with seawater-derived hydrothermal fluids may be a potential source for the MTZ chromitites.

The second stage is prograde metamorphic recrystallization of this hydrous mantle protolith as recorded by the multiphase type 1, 2 and 2a and microcrystal type 3

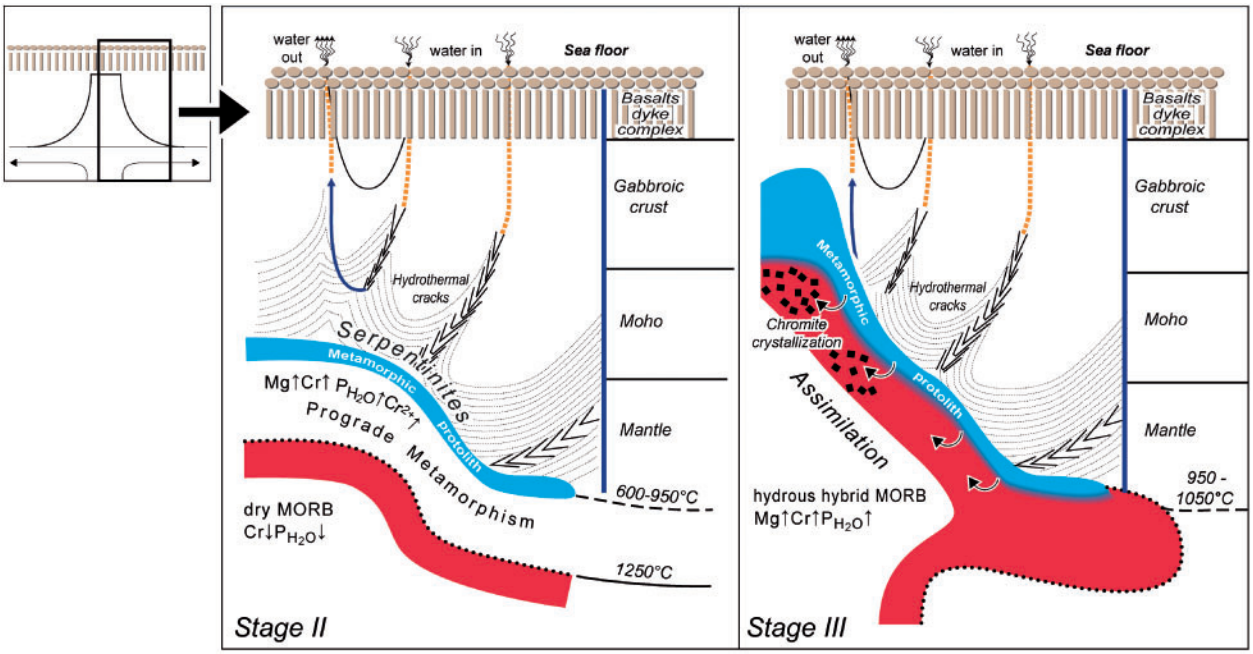

Fig. 8. Three-stage model of chromitite formation through assimilation of a metamorphic mantle protolith by MORB. Stages correspond to those in Table 3. Stage I is not shown in the figure. Stage II: during the uprise of an asthenospheric diapir, the overlying lithosphere is heated and serpentinized peridotite experiences prograde metamorphism. Reduced hydrothermal fluids (probably rich in Cr^{2+}) and the high Mg–Cr silicate minerals of the multiphase and microcrystal inclusions are generated in the thermal field of mantle upwelling above 600°C. Stage III: the metamorphic phases generated during stage II are assimilated by primitive MORB melts (initially poor in Cr and H_2O, and oxidized). The resultant hydrous hybrid MORB melt (enriched in Mg, Cr and H_2O) becomes oversaturated in chromite, leading to abundant chromite and chromite–olivine fractional crystallization in the MTZ. The process is responsible for the petrogenesis of the MTZ chromitites and dunites. The cooling was rapid owing to hydrothermal fluid circulation. After Benoit *et al.* (1999), Bosch *et al.* (2004) and Python *et al.* (2007).

and 6 inclusions (Table 3). High-Mg and -Cr silicate minerals in multiphase inclusions, pyroxenes and forsterite microcrystals in equilibrium with high cr-number chromite may be formed during this stage as a result of dehydration of the high-Mg and -Cr serpentinized protolith upon prograde metamorphism above 600°C. For example, the forsterite microcrystals may represent the dehydrated serpentine assemblage (e.g. Khedr & Arai, 2012). The Maqsad diapir (Fig. 8) channelled a large amount of rising MORB magma that produces the heat source in the contact aureole and the wall-rock serpentine dehydration during the second stage metamorphism. In addition to the mineral composition and inclusion data discussed above, our analyses of the oxygen isotope composition of the chromite ore bodies also support this scenario. The $\delta^{18}O$ values measured in the chromites (3·2–3·8‰) are consistent with the involvement of hydrothermal fluids derived either from seawater directly or from prograde dehydration of the protolith, which was originally altered by seawater-derived hydrothermal fluids during the initial stage (e.g. Alt *et al.*, 1996; Fruh-Green *et al.*, 2003). Indeed, calculation of the isotope composition of the aqueous fluid using the equilibrium $\Delta^{18}O$ values for the fractionation between chromite and water at 1000°C (Zheng, 1991) and the measured $\delta^{18}O$ of chromite (3·2–3·8‰) yields a $\delta^{18}O_{H2O}$ value of 7·9–8·5‰ for the aqueous fluid, typical for Cretaceous seawater-derived hydrothermal fluids associated with the Oman ophiolites (Gregory & Taylor, 1981).

The third stage, illustrated in Figs 7 and 8, occurred in the presence of a hydrous hybrid MORB melt as recorded by crystallization of the host chromite and late anhedral type 4 and 5 inclusions. The petrogenesis of the MTZ chromitites and host dunites during this stage is in accordance with Irvine's (1975) model applied to illustrate our model of assimilation of the metamorphic protolith into a MORB melt (Fig. 7). The resultant hydrous, hybrid MORB melt (enriched in Cr and H_2O) becames oversaturated in chromite, leading to abundant fractional crystallization of chromite in the MTZ. At this stage, the chromite grains could crystallize while the metamorphic protolith was being continuously assimilated. Cooling was rapid owing to the involvement of hydrothermal fluids and fractional crystallization was efficient. The observed textures of the MTZ chromitites suggest a melt- or fluid-saturated medium during the third stage and cumulative, possibly, convective control on the distribution of the minerals inside the crystallizing dykes (see Leblanc & Ceuleneer, 1992). Once formed, the host chromite crystals may be accumulated gravitationally in an ore body owing to their high density (~4500 kg m^{-3}; e.g. Mungall &

Naldrett, 2008) and may be sintered (Hulbert & von Gruenewaldt, 1985). The latter process may explain the absence of entrapped basaltic glass in the host chromite. Our oxygen isotope data also provide independent support for the third magmatic stage. The measured $\delta^{18}O$ values in chromite (3·2–3·8‰) in the Maqsad chromitites (Table 4) and associated olivine (5·2–5·8‰ in the Maqsad dunites) yield an average chromite–olivine oxygen isotopic fractionation ($\Delta^{18}O$) value of −2·0‰. This small fractionation is consistent with equilibrium isotope fractionation at high temperatures of 1050°C, calculated using a combination of available $\delta^{18}O$ fractionation in the pairs chromite–water (Zheng, 1991), basalt–water and olivine–basalt (Zhao & Zheng, 2003). If the total range of $\Delta^{18}O$ (olivine–spinel) = 1·4–2·6‰ that we observe between chromitites and associated dunite is considered, this would correspond to temperatures higher that 600°C. This indicates that although the involved protolith had a high $\delta^{18}O$, perhaps because of alteration by seawater during the first stage at lower temperature, the later prograde metamorphism and magmatic stages variably equilibrated olivine and chromite with respect to their $\delta^{18}O$ values.

The proposed model for MTZ chromitite genesis extends our knowledge of physicochemical processes occurring during MORB transport at Moho-level depths. The metamorphic mantle protolith would supply H_2O, S, Cl and Na to the primitive MORB melts (Bédard *et al.*, 2000; and references therein). The saturation of the MORB melts with a C–O–H–Cl–S fluid would have played a key role in the MTZ chromitite formation. The presence of a deep metamorphic source and its impact on the MORB melt chemistry is thus consistent with the growing evidence for (1) oceanic lithosphere assimilation by MORB, and the petrogenesis of evolved lithospheric magmas in the mid-ocean ridges (e.g. Nonnotte *et al.*, 2005; Kamenetsky & Gurenko, 2007) and in geodynamically similar regions such as Iceland (Bindeman *et al.*, 2012), (2) abundance of MORB enriched in C–O–H fluids (e.g. Javoy & Pineau, 1991), and (3) ubiquity of chromitite ores found in the Moho Transition Zone of ophiolite massifs over the world.

CONCLUSIONS

The results of systematic analyses, carried out in this study, of chromite-hosted inclusions as well as oxygen isotopes of chromite grain fractions from nodular, disseminated and stratiform chromitites and associated host dunites that are located at different levels of the MTZ in the Oman ophiolite (Maqsad area) are consistent with a three-stage model of the chromitite petrogenesis in which most of the Maqsad MTZ chromitites crystallized at temperatures between 600°C and 1050°C and pressures of 200 MPa. In the first stage, a mantle protolith altered by seawater-derived hydrothermal fluids yielded serpentinites and serpentinized harzburgites, which were probably the main source of chromium for chromitite ore at the Moho level and explain the systematically high Mg/Fe ratios of the silicate minerals found in the ophiolite chromitites. The presence of such hydrous mantle protolith thus eliminates the existing controversy on the source of Cr and H_2O and its role in the chromitite petrogenesis. The second stage involved subsolidus (metamorphic) crystallization at 600–950°C. It was followed by a third stage of assimilation and fractional crystallization of chromite from water-saturated MORB at 950–1050°C in the oceanic ridge setting. The assimilation of this protolith at Moho-level depths dramatically affected the MORB magma chemistry and favored Cr concentration into economic ores. Our model is supported by the growing evidence for oceanic lithosphere assimilation by MORB, abundance of hydrous MORB enriched in C–O–H fluids and ubiquity of chromitite ore deposits in the Moho Transition Zone observed in ophiolite massifs world-wide.

ACKNOWLEDGEMENTS

We dedicate this work to the memory of Leonid V. Dmitriev, who was a great personality and scientist probing the ocean depths in numerous Russian Academy of Science, Deep Sea Drilling Program (DSDP) and Ocean Drilling Program cruises. We thank editors G. Woerner and M. Wilson, and H. Rollinson, J. Natland, R. Almeev, J. Bédard, F. Melcher, F. Costa and several anonymous referees for editorial corrections and very constructive reviews. M. Grégoire, K. Kouzmanov, C. Li and M. Python are acknowledged for their help during preparation of the manuscript. Ch. Cavare-Hester is thanked by A.Y.B. for great help in figure design. We are grateful to S. Matveev for providing us with unpublished data. We thank J. F. Mena for sample preparation. V. Yapaskurt is thanked for X-ray imaging (Moscow State University). C. Ballhaus, B. Bazylev, M. Benoit, A. Bychkov, A. Delacour, F. Faure, S. Feig, D. Jousselin, J. Koepke, G. Nikolaev, M. and D. Ohnenstetter, M. Pichavant, M. Portnyagin, C. Ramboz, L. Reisberg, O. Safonov, B. Scaillet, P. Schiano, K. Schmulovitch, M. Toplis, L. Truche and M. Yudovskaya are thanked for insightful discussions. We are extremely grateful to J. Prunier for assistance during the leaching procedure at GET (France), and to J. Palandri for oxygen isotope measurements at the University of Oregon (USA).

FUNDING

This work was supported by a CNRS grant 'Poste Rouge' to A.Y.B. and French–Japanese linkage grant PHC-Sakura 21225NG. The work was supported by grants from RFBR (10-05-00254-a, Russia, 2010–2012), INSU ('CHROMAN', France, 2010–2011) and OMP (Observatoire Midi-Pyrenees, France, 2011–2012). V.K. was

supported by the Australian Research Council, the University of Tasmania and the Russian Ministry of Science and Education (grant 2012-1.5-12-000-1006-001).

SUPPLEMENTARY DATA

Supplementary data for this paper are available at *Journal of Petrology* online.

REFERENCES

Abily, B., Ceuleneer, G. & Launeau, P. (2011). Synmagmatic normal faulting in the lower crust: Evidence from the Oman ophiolite. *Geology* **39**, 391–394.

Abily, B. & Ceuleneer, G. (in press). The dunitic mantle/crust transition zone in the Oman ophiolite: Residue of melt rock interaction, cumulates from high-MgO melts or both? *Geology*, in press.

Adam, J. & Green, T. H. (1994). The effect of pressure and temperature on the partitioning of Ti, Sr and REE between amphibole, clinopyroxene and basanitic melts. *Chemical Geology* **117**, 219–233.

Ahmed, A. H., Hahghøj, K., Kelemen, P. B., Hart, S. R. & Arai, S. (2006). Osmium isotope systematics of the Proterozoic and Phanerozoic ophiolitic chromitites: *In situ* ion probe analysis of primary Os-rich PGM. *Earth and Planetary Science Letters* **245**, 777–791.

Alt, J. C., Laverne, C., Vanko, D. A., Tartarotti, P., Teagle, D. A. H., Bach, W., Zuleger, E., Erzinger, J., Honnorez, J., Pezard, P. A., Becker, K., Salisbury, M. H. & Wilkens, R. H. (1996). Hydrothermal alteration of a section of upper oceanic crust in the Eastern Equatorial Pacific: A synthesis of results from site 504 (DSDP Legs 69, 70, and 83, and ODP legs 111, 137, 140, and 148). In:? In: Alt, J. C., Kinoshita, H., Stokking, L. B. & Michael, P. J. (eds) *Proceeding of the Ocean Drilling Program. Scientific Results, 148.* College Station, TX: Ocean Drilling Program, pp. 417–434.

Amri, I., Benoit, M. & Ceuleneer, G. (1996). Tectonic setting for the genesis of oceanic plagiogranites: evidence from a paleo-spreading structure in the Oman ophiolite. *Earth and Planetary Science Letters* **139**, 177–194.

Arai, S. & Takemoto, Y. (2007). Mantle wehrlite from Hess Deep as a crystal cumulate from an ultra-depleted primary melt in East Pacific Rise. *Geophysical Research Letters* **34**, L08302.

Arai, S., Uesugi, J. & Ahmed, A. H. (2004). Upper crustal podiform chromitite from the northern Oman ophiolite as the stratigraphically shallowest chromitite in ophiolite and its implication for Cr concentration. *Contributions to Mineralogy and Petrology* **147**, 145–154.

Arai, S., Kadoshima, K. & Morishita, T. (2006). Widespread arc-related melting in mantle section of the northern Oman ophiolite as inferred from detrital chromian spinels. *Journal of the Geological Society, London* **163**, 1–11.

Arai, S., Okamura, H., Kadoshima, K., Tanaka, C., Suzuki, K. & Ishimaru, S. (2011). Chemical characteristics of chromian spinel in plutonic rocks: Implications for deep magma processes and discrimination of tectonic setting. *Island Arc* **20**, 125–137.

Asimow, P. D. & Langmuir, C. H. (2003). The importance of water to oceanic mantle melting regimes. *Nature* **421**, 815–820.

Augé, T. (1987). Chromite deposits in the Northern Oman ophiolite: mineralogical constraints. *Mineralium Deposita* **22**, 1–10.

Augé, T. & Johan, Z. (1988). Comparative study of chromite deposits from Troodos, Vourinos, North Oman and New Caledonia ophiolites. In: Boissonnas, J. & Omenetto, P. (eds) *Mineral Deposits within the European Community.* Berlin: Springer, pp. 267–288.

Ballhaus, C., Berry, R. F. & Green, D. H. (1990). Oxygen fugacity controls in the Earth's upper mantle. *Nature* **348**, 437–440.

Ballhaus, C., Berry, R. F. & Green, D. H. (1991). High pressure experimental calibration of the olivine–orthopyroxene–spinel oxygen geobarometer: implications for the oxidation state of the upper mantle. *Contributions to Mineralogy and Petrology* **107**, 27–40.

Barnes, S. J. & Roeder, P. L. (2001). The range of spinel compositions in terrestrial mafic and ultramafic rocks. *Journal of Petrology* **42**, 2279–2302.

Bédard, J. H. & Hébert, R. (1998). Formation of chromitites by assimilation of crustal pyroxenites and gabbros into peridotitic intrusions: North Arm Mountain Massif, Bay of Islands ophiolite, Newfoundland, Canada. *Journal of Geophysical Research* **103**, 5165–5184.

Bédard, J. H., Hébert, R., Berclas, A. & Varfalvy, V. (2000). Syntexis and genesis of lower oceanic crust. In: Dilek, Y., Moores, E. M., Elthon, D. & Nicolas, A. (eds) *Ophiolites and Oceanic Crust: New Insights from Field Studies and Ocean Drilling Program. Geological Society of America, Special Papers* **349**, 105–119.

Bédard, J. H., Pagé, P., Bécu, V., Schroetter, J.-M. & Tremblay, A. (2007). Overview of the geology and Cr–PGE potential of the Southern Québec ophiolite belt. In: Goodfellow, W. D. (ed.) *Mineral Deposits of Canada: A Synthesis of Major Deposit-types, District Metallogeny, the Evolution of Geological Provinces, and Exploration Methods. Geological Association of Canada, Mineral Deposits Division, Special Publications* **5**, 433–448.

Béjina, F., Sautter, V. & Jaoul, O. (2009). Cooling rate of chondrules in ordinary chondrites revisited by a new geospeedometer based on the compensation rule. *Physics of the Earth and Planetary Interiors* **172**, 5–12.

Benoit, M., Ceuleneer, G. & Polvé, M. (1999). The remelting of hydrothermally altered peridotite at mid-ocean ridges by intruding mantle diapirs. *Nature* **402**, 514–518.

Berndt, J., Koepke, J. & Holtz, F. (2005). An experimental investigation of the influence of water and oxygen fugacity on differentiation of MORB at 200 MPa. *Journal of Petrology* **46**, 135–167.

Bindeman, I. N. (2008). Oxygen isotopes in mantle and crustal magmas as revealed by single crystal analysis. In: Putirka, K. D. & Tepley, F. J., III (eds) *Minerals, Inclusions and Volcanic Processes. Mineralogical Society of America and Geochemical Society, Reviews in Mineralogy and Geochemistry* **69**, 445–478.

Bindeman, I. N., Gurenko, A., Carley, T., Miller, C., Martin, E. & Sigmarsson, O. (2012). Silicic magma petrogenesis in Iceland by remelting of hydrothermally altered crust based on oxygen isotope diversity and disequilibria between zircon and magma with implications for MORB. *Terra Nova* **24**, 227–232.

Borisova, A. Y., Portnyagin, M. V., Sushchevskaya, N. M., Tsekhonya, T. I. & Kononkova, N. N. (1997). Olivine basalts of the Afanasij Nikitin Rise, Indian Ocean: Petrology and deuteric alteration. *Geochemistry International* **35**, 346–358.

Borisova, A. Y., Belyatsky, B. V., Portnyagin, M. V. & Sushchevskaya, N. M. (2001). Petrogenesis of olivine-phyric basalts from the Aphanasey Nikitin Rise: Evidence for contamination by cratonic lower continental crust. *Journal of Petrology* **42**, 277–319.

Borisova, A. Y., Nikogosian, I. K., Scoates, J., Weis, D., Damasceno, D., Shimizu, N. & Touret, J. L. R. (2002). Melt, fluid and crystal inclusions in olivine phenocrysts from Kerguelen plume-derived picritic basalts: Evidence for interaction with the Kerguelen Plateau lithosphere. *Chemical Geology* **183**, 195–220.

Borisova, A. Y., Ceuleneer, G., Arai, S., Bejina, F., Bazylev, B. A. & Polvé, M. (2008). Inclusions and crown-like chrome spinel in chromitites from the Oman ophiolite: Evidence for hydrous MORB melts in the mantle–crust transition zone. *Geochimica et Cosmochimica Acta, Supplement 1* **72**, A98.

Borisova, A. Y., Pokrovski, G. S., Pichavant, M., Freydier, R. & Candaudap, F. (2010). Arsenic enrichment in hydrous peraluminous melts: insights from LA-ICPMS and *in situ* X-ray absorption spectroscopy. *American Mineralogist* **95**, 1095–1104.

Bosch, D., Jamais, M., Boudier, F., Nicolas, A., Dautria, J. M. & Agrinier, P. (2004). Deep and high-temperature hydrothermal circulation in the Oman ophiolite—petrological and isotopic evidence. *Journal of Petrology* **45**, 1181–1208.

Boudier, F., Bouchez, J.-L., Nicolas, A., Cannat, M., Ceuleneer, G., Misseri, M. & Montigny, M. (1985). Kinematics of oceanic thrusting in the Oman ophiolite. Model of plate convergence. *Earth and Planetary Science Letters* **75**, 215–222.

Boudier, F., Ceuleneer, G. & Nicolas, A. (1988). Shear zones, thrusts and related magmatism in the Oman ophiolite: initiation of thrusting on an oceanic ridge. *Tectonophysics* **151**, 275–296.

Brearley, M. & Scarfe, C. M. (1986). Dissolution rates of upper mantle minerals in an alkali basalt melt at high pressure—an experimental study and implications for ultramafic xenolith survival. *Journal of Petrology* **27**, 1157–1182.

Clénet, H., Ceuleneer, G., Pinet, P., Abily, B., Daydou, Y., Harris, E., Amri, I. & Dantas, C. (2010). Thick sections of layered ultramafic cumulates in the Oman ophiolite revealed by an airborne hyperspectral survey: petrogenesis and relationship to mantle diapirism. *Lithos* **114**, 265–281.

Coleman, R. G. (1981). Tectonic setting for ophiolite obduction in Oman. *Journal of Geophysical Research* **86**, 2497–2508.

Costa, F., Dungan, M. A. & Singer, B. S. (2001). Magmatic Na-rich phlogopite in a suite of gabbroic crustal xenoliths from Volcán San Pedro, Chilean Andes: Evidence for a solvus relation between phlogopite and aspidolite. *Americal Mineralogist* **86**, 29–35.

Crerar, D., Wood, S. & Brantley, S. (1985). Chemical controls on solubility of ore-forming minerals in hydrothermal solutions. *Canadian Mineralogist* **23**, 333–352.

Danyushevsky, L. V., Sobolev, A. V. & Dmitriev, L. V. (1996). Estimation of the pressure of crystallization and H_2O content of MORB and BABB glasses: calibration of an empirical technique. *Mineralogy and Petrology* **57**, 185–204.

Danyushevsky, L. V., Sokolov, S. & Falloon, T. J. (2002). Melt inclusions in olivine phenocrysts: using diffusive re-equilibration to determine the cooling history of a crystal, with implications for the origin of olivine-phyric volcanic rocks. *Journal of Petrology* **43**, 1651–1671.

Deer, W. A., Howie, R. A. & Zussman, J. (1997). *Rock-forming Minerals. Orthosilicates. Volume 1A*. London: Geological Society, 919 p.

Dick, H. J. B. & Bullen, T. (1984). Chromian spinel as petro-genetic indicator in abyssal and alpine-type peridotites and spatially associated lavas. *Contributions to Mineralogy and Petrology* **86**, 54–76.

Dunn, T. (1987). Partitioning of Hf, Lu, Ti and Mn between olivine, clinopyroxene and basaltic liquid. *Contributions to Mineralogy and Petrology* **96**, 476–484.

Feig, S. T., Koepke, J. & Snow, J. E. (2006). Effect of water on tholeiitic basalt phase equilibria: an experimental study under oxidizing conditions. *Contributions to Mineralogy and Petrology* **152**, 611–638.

Ford, C. E., Biggar, G. M., Humphries, D. J., Wilson, G., Dixon, D. & O'Hara, M. J. (1972). Role of water in the evolution of the lunar crust; an experimental study of sample 14310; an indication of lunar calc-alkaline volcanism. *Proceedings of 3rd Lunar Scientific Conference. Geochimica et Cosmochimica Acta* Supplement 3: 207–229.

Fruh-Green, G. L., Kelley, D. S., Bernasconi, S. M., Karson, J. A., Ludwig, K. A., Butterfield, D. A., Boschi, C. & Proskurowski, G. (2003). 30,000 years of hydrothermal activity at the Lost City vent field. *Science* **301**, 495–498.

Ganguly, J., Yang, H. & Ghose, S. (1994). Thermal history of mesosiderites: Quantitative constraints from compositional zoning and Fe–Mg ordering in orthopyroxenes. *Geochimica et Cosmochimica Acta* **58**, 2711–2723.

Ghent, E. D. & Stout, M. Z. (1981). Metamorphism at the base of the Samail ophiolite, Southeastern Oman Mountains. *Journal of Geophysical Research* **86**, 2557–2571.

Glennie, K. W., Boeuf, M. G. A., Hughes-Clark, M. W., Moody-Stuart, M., Pilaar, W. F. H. & Reinhardt, B. M. (1973). Late Cretaceous nappes in Oman mountains and their geologic evolution. *AAPG Bulletin* **57**, 5–27.

Gregory, R. T. & Taylor, H. P., Jr (1981). An oxygen isotope profile in a section of Cretaceous oceanic crust, Samail ophiolite, Oman: Evidence for $\delta^{18}O$ buffering of the oceans by deep (>5 km) seawater–hydrothermal circulation at mid-ocean ridges. *Journal of Geophysical Research* **86**, 2737–2755.

Hanson, B. & Jones, J. H. (1998). The systematics of Cr^{3+} and Cr^{2+} partitioning between olivine and liquid in the presence of spinel. *American Mineralogist* **83**, 669–684.

Hart, S. R. & Dunn, T. (1993). Experimental cpx/melt partitioning of 24 trace elements. *Contributions to Mineralogy and Petrology* **113**, 1–8.

Holland, T. & Blundy, J. (1994). Non-ideal interactions in calcic amphiboles and their bearing on amphibole–plagioclase thermobarometry. *Contributions to Mineralogy and Petrology* **116**, 433–447.

Hulbert, L. J. & von Gruenewaldt, G. (1985). Textural and compositional features of chromite in the Lower and Critical Zones of the Bushveld Complex south of Potgietersrus. *Economic Geology* **80**, 872–895.

Irvine, T. N. (1975). Crystallization sequences in the Muskox intrusion and other layered intrusions—II. Origin of chromitite layers and similar deposits of other magmatic ores. *Geochimica et Cosmochimica Acta* **39**, 991–1020.

Jackson, E. D. (1966). Liquid immiscibility in chromite seam formation—a discussion. *Economic Geology* **61**, 777–780.

Javoy, M. & Pineau, F. (1991). The volatiles record of 'popping' rock from the Mid-Atlantic Ridge at 14°N: chemical and isotopic composition of gas trapped in the vesicles. *Earth and Planetary Science Letters* **107**, 598–611.

Johan, Z. & Le Bel, L. (1978). Sur la genèse des couches et podes de chromite dans les complexes ophiolitiques. *Résumé des principaux résultats science et technique. Service Géologique National*. Paris, France: Supplément au bulletin B.R.G.M., 96–99.

Johan, Z., Dunlop, H., Le Bel, L., Robert, J. L. & Volfinger, M. (1983). Origin of chromite deposits in ophiolitic complexes: evidence for a volatile- and sodium-rich reducing fluid phase. *Fortschritte der Mineralogie* **61**, 105–107.

Jousselin, D., Nicolas, A. & Boudier, F. (1998). Detailed mapping of a mantle diapir below a paleo-spreading center in the Oman ophiolite. *Journal of Geophysical Research* **103**, 18153–18170.

Kamenetsky, V. S. (1996). Methodology for the study of melt inclusions in Cr-spinel, and implications for parental melts of MORB from FAMOUS area. *Earth and Planetary Science Letters* **142**, 479–486.

Kamenetsky, V. S. & Gurenko, A. A. (2007). Cryptic crustal contamination of MORB primitive melts recorded in olivine-hosted glass and mineral inclusions. *Contributions to Mineralogy and Petrology* **153**, 465–481.

Kamenetsky, V. S., Crawford, A. J. & Meffre, S. (2001). Factors controlling chemistry of magmatic spinel: an empirical study of associated olivine, Cr-spinel and melt inclusions from primitive rocks. *Journal of Petrology* **42**, 655–671.

Kamenetsky, V. S., Sobolev, A. V., Eggins, S. M., Crawford, A. J. & Arculus, R. J. (2002). Olivine-enriched melt inclusions in chromites from low-Ca boninites, Cape Vogel, Papua New Guinea: evidence

for ultramafic primary magma, refractory mantle source and enriched components. *Chemical Geology* **183**, 287–303.

Kelemen, P. B., Shimizu, N. & Salters, V. J. M. (1995). Extraction of mid-ocean-ridge basalt from the upwelling mantle by focused flow of melt in dunite channels. *Nature* **375**, 747–753.

Khedr, M. Z. & Arai, S. (2012). Petrology and geochemistry of prograde deserpentinized peridotites from Happo-O'ne, Japan: Evidence of element mobility during deserpentinization. *Journal of Asian Sciences* **43**, 150–163.

Koepke, J., Berndt, J., Feig, S. T. & Holtz, F. (2007). The formation of SiO_2-rich melts within the deep oceanic crust by hydrous partial melting of gabbros. *Contributions to Mineralogy and Petrology* **153**, 67–84.

Koepke, J., Berndt, J., Feig, S. T. & Holtz, F. (2009). Petrogenesis of crustal wehrlites in the Oman ophiolite: Experiments and natural rocks. *Geochemistry, Geophysics, Geosystems* **10**, doi:10.1029/2009GC002488.

Korenaga, J. & Kelemen, P. B. (1997). Origin of gabbro sills in the Moho transition zone of the Oman ophiolite: implications for magma transport in the oceanic lower crust. *Journal of Geophysical Research* **102**, 27729–27749.

Lago, B. L., Rabinowicz, M. & Nicolas, A. (1982). Podiform chromite ore bodies: a genetic model. *Journal of Petrology* **23**, 103–125.

LaTourette, T., Hervig, R. L. & Holloway, J. R. (1995). Trace element partitioning between amphibole, phlogopite, and basanite melt. *Earth and Planetary Science Letters* **135**, 13–30.

Leblanc, M. & Ceuleneer, G. (1992). Chromite crystallization in a multicellular magma flow: evidence from a chromitite dike in the Oman ophiolite. *Lithos* **27**, 231–257.

Lehnert, K., Su, Y., Langmuir, C. H., Sarbas, B. & Nohl, U. (2000). A global geochemical database structure for rocks. *Geochemistry, Geophysics, Geosystems* **1(5)**, doi:10.1029/1999GC000026.

Li, C., Ripley, E. M., Sarkar, A., Shin, D. & Maier, W. D. (2005). Origin of phlogopite–orthopyroxene inclusions in chromites from the Merensky Reef of the Bushveld Complex, South Africa. *Contributions to Mineralogy and Petrology* **150**, 119–130, doi:10.1007/s00410-005-0013-z.

Li, Z.-X. A. & Lee, C.-T. A. (2006). Geochemical investigation of serpentinized oceanic lithospheric mantle in the Feather River Ophiolite, California: Implications for the recycling rate of water by subduction. *Chemical Geology* **235**, 161–185.

Lorand, J. P. (1987). A new occurrence of native iron in serpentinized mantle peridotite—Maqsad, Sumail Massif, Semail Ophiolite (Southern Oman). *Comptes Rendus de l'Académie des Sciences, Série II* **304**, 703–706.

Lorand, J. P. & Ceuleneer, G. (1989). Silicate and base-metal sulphide inclusions in chromites from the Maqsad area (Oman ophiolite, Gulf of Oman): a model for entrapment. *Lithos* **22**, 173–190.

Manning, C. E., Wilke, M., Schmidt, C. & Cauzid, J. (2008). Rutile solubility in albite–H_2O and $Na_2Si_3O_7$–H_2O at high temperatures and pressures by *in-situ* synchrotron radiation micro-XRF. *Earth and Planetary Science Letters* **272**, 730–737.

Mattey, D., Lowry, D. & Macpherson, C. (1994). Oxygen-isotope composition of mantle peridotite. *Earth and Planetary Science Letters* **128**, 231–234.

Matveev, S. & Ballhaus, C. (2002). Role of water in the origin of podiform chromitite deposits. *Earth and Planetary Science Letters* **203**, 235–243.

Maurel, C. & Maurel, P. (1982*a*). Etude expérimentale de la solubilité du chrome dans les bains silicatés basiques et de sa distribution entre liquide et minéraux coexistants Conditions d'existence du spinelle chromifère. *Bulletin Minéralogique* **105**, 640–647.

Maurel, C. & Maurel, P. (1982*b*). Etude expérimentale de la distribution de l'aluminium entre bain silicaté basique et spinelle chromifère. Implications pétrogénétiques: teneur en chrome des spinelles. *Bulletin Minéralogique* **105**, 197–202.

Maurel, C. & Maurel, P. (1982*c*). Etude expérimentale de l'équilibre Fe^{2+}–Fe^{3+} dans les spinelles chromifères et les liquides silicatés basiques coexistantes. *Comptes Rendus de l'Académie des Sciences* **295**, 209–212.

McDonald, J. A. (1965). Liquid immiscibility as factor in chromitite seam formation in the Bushveld igneous complex. *Economic Geology* **60**, 1674–1685.

Melcher, F., Grum, W., Simon, G., Thalhammer, T. V. & Stumpfl, E. F. (1997). Petrogenesis of the ophiolitic giant chromite deposits of Kempirsai, Kazakhstan: a study of solid and fluid inclusions in chromite. *Journal of Petrology* **38**, 1419–1458.

Montigny, R., Le Mer, O., Thuizat, R. & Whitechurch, H. (1988). K–Ar and $^{40}Ar/^{39}Ar$ study of metamorphic rocks associated with the Oman ophiolite: tectonic implications. *Tectonophysics* **151**, 345–362.

Mungall, J. E. & Naldrett, A. J. (2008). Ore deposits of the platinum-group elements. *Elements* **4**, 253–258.

Muntener, O., Kelemen, P. B. & Grove, T. L. (2001). The role of H_2O during crystallization of primitive arc magmas under uppermost mantle conditions and genesis of igneous pyroxenites: an experimental study. *Contributions to Mineralogy and Petrology* **141**, 643–658.

Murck, B. W. & Campbell, I. H. (1986). The effect of temperature, oxygen fugacity and melt composition on the behaviour of chromium in basic and ultrabasic melts. *Geochimica et Cosmochimica Acta* **50**, 1871–1887.

Nicholson, D. M. & Mathez, E. A. (1991). Petrogenesis of the Merensky reef in the Rutherburg section of the Bushveld complex. *Contributions to Mineralogy and Petrology* **107**, 293–309.

Nonnotte, P., Ceuleneer, G. & Benoit, M. (2005). Genesis of andesitic–boninitic magmas at mid-ocean ridges by melting of hydrated peridotites: geochemical evidence from DSDP Site 334 gabbronorites. *Earth and Planetary Science Letters* **236**, 632–653.

O'Neill, H. St. C. & Wall, V. J. (1987). The olivine–orthopyroxene–spinel oxygen geobarometer, the nickel precipitation curve, and the oxygen fugacity of the Earth's upper mantle. *Journal of Petrology* **28**, 1169–1191.

Onuma, K. & Tohara, T. (1981). Clinopyroxenes and spinels in the system $CaMgSi_2O_6$–$CaAl_2SiO_6$–$CaCrAlSiO_6$; a preliminary report. *Journal of the Faculty of Science, Hokkaiodo University* **19**, 495–501.

Pagé, Ph., Bédard, J. H., Schroetter, J.-M. & Tremblay, A. (2008). Mantle petrology and mineralogy of the Thetford Mines Ophiolite Complex. *Lithos* **100**, 255–292.

Pearce, J. A., Alabaster, T., Shelton, A. W. & Searle, M. P. (1981). The Oman ophiolite as a Cretaceous arc–basin complex: evidence and implications. *Philosophical Transactions of the Royal Society of London* **300**, 299–317.

Pokrovski, G. S., Schott, J., Hazemann, J.-L., Farges, F. & Pokrovsky, O. S. (2002). An X-ray absorption fine structure and nuclear magnetic resonance spectroscopy study of gallium–silica complexes in aqueous solution. *Geochimica et Cosmochimica Acta* **66**, 4203–4322.

Pokrovski, G. S., Schott, J., Farges, F. & Hazemann, J.-L. (2003). Iron(III)–silica interactions in aqueous solution: Insights from X-ray absorption fine structure spectroscopy. *Geochimica et Cosmochimica Acta* **67**, 3559–3573.

Presnall, D. C. (1995). Phase diagrams of earth-forming minerals. In: Ahrens, T. J. (ed.) *Mineral Physics and Crystallography: A Handbook of*

Physical Constants (AGU Reference Shelf). Washington, DC: American Geophysical Union, pp. 248–268.

Pushkarev, E. V., Anikina, E. V., Garuti, G. & Zakkarini, F. (2007). Chrome–platinum deposit of Nizhnetagilsky type on Ural: Structure and compositional characteristics and petrogenetic problem. *Lithosphere* **3**, 28–65 (in Russian).

Python, M. & Ceuleneer, G. (2003). Nature and distribution of dykes and related melt migration structures in the mantle section of the Oman ophiolite. *Geochemistry, Geophysics, Geosystems* **4(7)**, 8612, doi:10.1029/2002GC000354.

Python, M., Ceuleneer, G., Ishida, Y., Barrat, J.-A. & Arai, S. (2007). Oman diopsidites: a new lithology diagnostic of very high temperature hydrothermal circulation in mantle peridotite below oceanic spreading centres. *Journal of Mineralogical and Petrological Sciences* **102**, 143–149.

Python, M., Ceuleneer, G. & Arai, S. (2008). Cr-spinel in mafic–ultramafic mantle dykes: evidence for a two-stage melt production during the evolution of the Oman ophiolite. *Lithos* **106**, 137–154.

Rabinowicz, M. & Ceuleneer, G. (2005). The effect of sloped isotherms on melt migration in the shallow mantle: a physical and numerical model based on observations in the Oman ophiolite. *Earth and Planetary Science Letters* **229**, 231–246.

Roeder, P. L. & Reynolds, I. (1991). Crystallization of chromite and chromium solubility in basaltic melts. *Journal of Petrology* **32**, 909–934.

Rollinson, H. (2008). The geochemistry of mantle chromitites from the northern part of the Oman ophiolite: inferred parental melt compositions. *Contributions to Mineralogy and Petrology* **156**, 273–288, doi:10.1007/s00410-008-0284-2.

Sachan, H. K., Mukherjee, B. K. & Bodnar, R. L. (2007). Preservation of methane generated during serpentinization of upper mantle rocks: Evidence from fluid inclusions in the Nidar ophiolite, Indus Suture Zone, Ladakh (India). *Earth and Planetary Science Letters* **257**, 47–59.

Sack, R. O. & Ghiorso, M. S. (1991). Chromian spinel as petrogenetic indicators: thermodynamics and petrological applications. *American Mineralogist* **76**, 827–847.

Schiano, P., Clocchiatti, R., Lorand, J.-P., Massare, D., Deloule, E. & Chaussidon, M. (1997). Primitive basaltic melt included in podiform chromites from the Oman Ophiolite. *Earth and Planetary Science Letters* **146**, 489–497.

Schmitt, A. K., Perfit, M. R., Rubin, K. H., Stockli, D. F., Smith, M. C., Cotsonika, L. A., Zellmer, G. F., Ridley, W. I. & Lovera, O. M. (2011). Rapid cooling rates at an active mid-ocean ridge from zircon thermochronology. *Earth and Planetary Science Letters* **302**, 349–358.

Scowen, P. A. H., Roeder, P. L. & Helz, R. T. (1991). Reequilibration of chromite within Kilauea Iki lava lake, Hawaii. *Contributions to Mineralogy and Petrology* **107**, 8–20.

Searle, M. & Cox, J. (1999). Tectonic setting, origin, and obduction of the Oman ophiolite. *Geological Society of America Bulletin* **111**, 104–122.

Shimizu, K., Komiya, T., Hirose, K., Shimizu, N. & Matuyama, S. (2001). Cr-spinel, an excellent micro-container for retaining primitive melt—implications for a hydrous plume origin for komatiites. *Earth and Planetary Science Letters* **189**, 177–188.

Shock, E. L., Sassani, D.C., Willis, M. & Sverjensky, D. A. (1997). Inorganic species in geologic fluids: Correlations among standard molal thermodynamic properties of aqueous ions and hydroxide complexes. *Geochimica et Cosmochimica Acta* **61**, 907–950.

Sigurdsson, I. A., Kamenetsky, V. S., Crawford, A. J., Eggins, S. M. & Zlobin, S. K. (1993). Primitive island arc and oceanic lavas from the Hunter Ridge–Hunter Fracture Zone. Evidence from glass, olivine and spinel compositions. *Mineralogy and Petrology* **47**, 149–169.

Skulski, T., Minarik, W. & Watson, E. B. (1994). High-pressure experimental trace-element partitioning between clinopyroxene and basaltic melts. *Chemical Geology* **117**, 127–147.

Snow, J. E., Hart, S. R. & Dick, H. J. B. (1994). Nd and Sr isotope evidence linking mid-ocean-ridge basalts and abyssal peridotites. *Nature* **371**, 57–60.

Spandler, C., Mavrogenes, J. & Arculus, R. (2005). Origin of chromitites in layered intrusions: Evidence from chromite-hosted melt inclusions from the Stillwater Complex. *Geology* **33**, 893–896.

Suzuki, A. M., Yasuda, A. & Ozawa, K. (2008). Cr and Al diffusion in chromite spinel: experimental determination and its implication for diffusion creep. *Physics and Chemistry of Minerals* **35**, 433–445.

Sverjensky, D. A., Shock, E. L. & Helgeson, H.C. (1997). Prediction of the thermodynamic properties of aqueous metal complexes to 1000°C and 5 kb. *Geochimica et Cosmochimica Acta* **61**, 1359–1412.

Tamura, A. & Arai, S. (2006). Harzburgite–dunite–orthopyroxenite suite as a record of supra-subduction zone setting for the Oman ophiolite mantle. *Lithos* **90**, 43–56.

Tilton, G. R., Hopson, C. A. & Wright, J. E. (1981). Uranium–lead isotopic ages of the Samail ophiolite, Oman with applications to Tethyan ocean ridge tectonics. *Journal of Geophysical Research* **86**, 2763–2775.

Tippit, P. R., Pessagno, E. A. & Smewing, J. D. (1981). The biostratigraphy of sediments in the volcanic unit of the Samail ophiolite. *Journal of Geophysical Research* **86**, 2756–2762.

VanTongeren, J. A., Kelemen, P. B. & Hanghøj, K. (2008). Cooling rates in the lower crust of the Oman ophiolite: Ca in olivine, revisited. *Earth and Planetary Science Letters* **267**, 69–82.

Wells, P. R. A. (1977). Pyroxene thermometry in simple and complex systems. *Contributions to Mineralogy and Petrology* **62**, 129–139.

Zhao, Z. F. & Zheng, Y. F. (2003). Calculations of oxygen isotope fractionation in magmatic rocks. *Chemical Geology* **193**, 59–80.

Zheng, Y. F. (1991). Calculation of oxygen isotope fractionation in metal oxides. *Geochimica et Cosmochimica Acta* **55**, 2299–2307.